J. Fluid Mech. (1996), *vol.* 322, *pp.* 21–49

Near-wake structure of an oscillating cylinder: effect of controlled shear-layer vortices

By C. K. CHYU AND D. ROCKWELL

Department of Mechanical Engineering and Mechanics, Lehigh University, Bethlehem, PA 18015, USA

(Received 16 May 1995 and in revised form 18 January 1996)

The instantaneous structure of the near wake of a cylinder subjected to small-amplitude perturbations is characterized using high-image-density particle image velocimetry. Emphasis is on control of the small-scale shear-layer vortices, which feed into the Kármán vortices. Modifications of the Kármán vortex formation are classified according to patterns of modulated and locked-on shear-layer vortices. The formation length of the Kármán vortices can be dramatically shortened and, in the limiting case, occur adjacent to the base of the cylinder when it is perturbed at the inherent instability frequency of the shear layer and its subharmonics. Moreover, the induced shear-layer vortices can lead to large-amplitude transverse undulations of the entire near-wake region during formation of the Kármán vortices.

These variations of the near-wake structure are further elucidated by considering the transient response of the wake, induced by abrupt cessation and onset of periodic motion of the cylinder. Distinctive intermediate states of the wake arise during relaxation to its asymptotic state; such relaxation requires a very large number of periods of the inherent instability of the shear layer.

1. Introduction

Schiller & Linke (1933) dramatically illustrated the sensitivity of the near wake of a cylinder over the range of Reynolds number from approximately 10^3 to 10^4. Small trip wires located near the onset of separation of the shear layer from the cylinder could induce substantial alterations in the extent of the 'dead zone' immediately downstream of the base of the cylinder. Since then, a wide range of insightful investigations have demonstrated the marked variations in the fluctuating lift coefficient $\tilde{C}_L$ and the pressure coefficient $-C_{pb}$ over this same range of Reynolds number. Comprehensive assessments of these variations of the overall loading on the cylinder are provided by Gerrard (1965), Roshko & Fiszdon (1969), McCroskey (1977), Zdravkovich (1988), Szepessy & Bearman (1992) and Williamson (1996). These features are, in turn, intimately related to the so-called vortex formation length. In essence, the decrease in formation length over the Reynolds number range $10^3 \leqslant Re \leqslant 10^4$ is in accord with increases in the magnitudes of $-C_{pb}$ and $\tilde{C}_L$. This formation length has been interpreted quantitatively by Bloor & Gerrard (1966) and Szepessy & Bearman (1992) using the streamwise variation of the characteristic velocity fluctuation. Alternatively, Unal & Rockwell (1988) employed a criterion based on a characteristic velocity fluctuation in the near wake.

Crucial to a proper interpretation of the sensitivity of the near wake is a detailed understanding of the unstable shear layers separating from the cylinder. Bloor (1964)

characterized the time-averaged features of the instability associated with the onset and development of small-scale vortices, including their predominant frequencies, and Gerrard (1965) emphasized the sensitivity of the unstable shear layer to free-stream disturbances, and thereby alteration of the time-mean characteristics of the very near wake. The overall features of the disturbed shear layer observed in these early studies are those of a shear-layer instability. This shear-layer instability is more appropriately described as a solution to the Rayleigh equation, which fully accounts for the distributed velocity and vorticity across the shear layer. For our present purposes, we designate the small-scale vortices formed in the layers separating from the cylinder as simply shear-layer vortices. The near wake therefore exhibits two coexisting modes: the shear-layer mode and the Kármán mode.

Bluff-body wakes are generally viewed as globally (absolutely) unstable in the Kármán mode (Huerre & Monkewitz 1990). Indeed, the robust, limit-cycle oscillations evident at low Reynolds number reinforce this view. There exists, however, a range of Re where the formation length of Kármán vortices is large. This increase in visualized formation length is accompanied by a decrease in the near-wake fluctuation level as Re is systematically increased from $Re \cong 200$ to $Re \cong 1000$ (Unal & Rockwell 1988).

The onset of the shear-layer vortices, which feed into the Kármán vortices, has been observed at different values of Reynolds number, extending from approximately 600 to 1900, no doubt due to variations in the level and spectral distribution of the incident free-stream turbulence, as well as possible upstream influence of the vortical structures in the near wake. Gerrard (1978), Wei & Smith (1986), Kourta *et al.* (1987), Unal & Rockwell (1988), Filler, Marston & Meih (1991), Ahmed, Khan & Bays-Muchmore (1993), Sheridan *et al.* (1993), Lin, Towfighi & Rockwell (1995), Chyu & Rockwell (1996) and Prasad & Williamson (1996) describe various aspects of both the quasi-two-dimensional and three-dimensional mechanisms of the unstable shear layer that feeds into the Kármán vortex. The potential for controlling the small-scale shear-layer vortices has been demonstrated in several investigations. Filler *et al.* (1991) show that the frequencies of excitation corresponding to maximum response of the near-wake velocity fluctuation are in good agreement with previous investigations of self-excited shear-layer instabilities from the corresponding stationary cylinder. Sheridan *et al.* (1993) demonstrate that peaks in the near-wake response are attainable at subharmonics of the inherent frequency of the shear-layer vortices and, furthermore, that the formation length of the Kármán vortices could be altered. Chyu *et al.* (1995) reveal that generation of phase-locked patterns of shear-layer vortices is particularly effective for inducing rapid onset of Kármán vortices.

The traditional approach to controlling the formation of Kármán vortices is to subject the cylinder to prescribed oscillations at frequencies slightly above and below the inherent Kármán frequency, and at amplitudes that are typically a substantial fraction of the cylinder diameter. For this type of excitation, a phase-locked response of the Kármán vortex formation relative to the cylinder motion is attainable, and drastic changes in timing of the initially shed vortex and mode of the near-wake vortex street can be induced as described by Zdravkovich (1982), Williamson & Roshko (1988), Öngoeren & Rockwell (1988), and Filler *et al.* (1991). Such control of the Kármán vortex formation is not limited to periodic excitation. Nakano & Rockwell (1993, 1994) demonstrate that amplitude- and frequency-modulated perturbations of the cylinder can give rise to a variety of phase-locked and modulated patterns of the Kármán vortices. The underlying motivation of these types of investigations is to assess the mechanisms of energy transfer between the fluid and the cylinder, which, in the corresponding elastically mounted system, would give rise to self-excited excitation. An

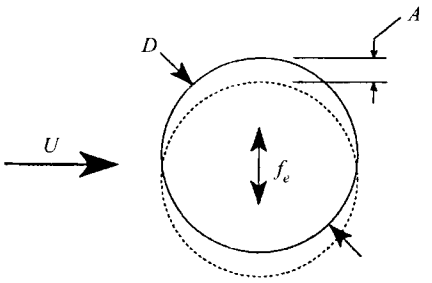

FIGURE 1. Schematic of the cylinder subjected to controlled oscillations.

important byproduct of such studies is an understanding of the mechanisms for enhancing mixing processes and convective heat transfer in the near-wake region.

In contrast, the present investigation aims to control *indirectly* the large-scale vortex formation by suitable manipulation of the small-scale shear-layer vortices. Excitation is at a frequency corresponding to the inherent instability frequency of the separating shear layer, or one of its subharmonics, and at amplitudes that are a small percentage of the cylinder diameter. Emphasis will be on the steady-state response of the near wake to these types of periodic excitation. In addition, transient excitation, corresponding to abrupt onset and cessation of the cylinder motion, will be invoked. Such excitation can induce a succession of states of the near wake, which involve remarkable alterations of the process of Kármán vortex formation. All these features will be characterized quantitatively using a technique of high-image-density particle image velocimetry, which provides the instantaneous velocity and vorticity distributions and the corresponding streamline patterns of the coexisting small- and large-scale vortical structures in the near wake.

2. Experimental system and techniques

Experiments were performed in a free-surface water channel having a test section 4880 mm long, a width of 914 mm, and a depth of 597 mm with the water level at 540 mm. A system of honeycomb screens produced a relatively low disturbance level of the free stream of less than 0.1%, with the major contributions to the spectral density of the kinetic energy at frequencies nearly two orders of magnitude smaller than the frequency of the shear layers from the cylinder. Figure 1 is a schematic of the cylinder subjected to controlled perturbations. Details of the cylinder mounting and forcing are described in detail by Chyu (1995). In essence, a cylinder of 51 mm diameter was mounted horizontally in the test section and connected by a vertical arm to a forcing system. A false wall–end plate arrangement ensured that only the two-dimensional cylinder was exposed to the flow. With this false wall arrangement in place, the effective width of the test section was 525 mm, giving an aspect ratio of $L/D = 10.3$, in which L is length and D is diameter. At a free-stream velocity of 91 mm s^{-1}, the Reynolds number was $Re = 5000$; higher values up to $Re = 10000$ were attained by increasing the free-stream velocity. The ratio of the inherent frequency f_i of the shear-layer instability to the frequency f_K of Kármán vortex formation is $f_i/f_K = 6.7$, representing well-separated length scales of the shear layer and Kármán modes. The onset of pronounced concentrations of vorticity in the shear layers separating from the cylinder was found to be influenced by the effective turbulence level of the free stream. At $Re = 5000$, experiments in a similar facility having a maximum intensity of 0.1% generated somewhat earlier onset of pronounced vorticity

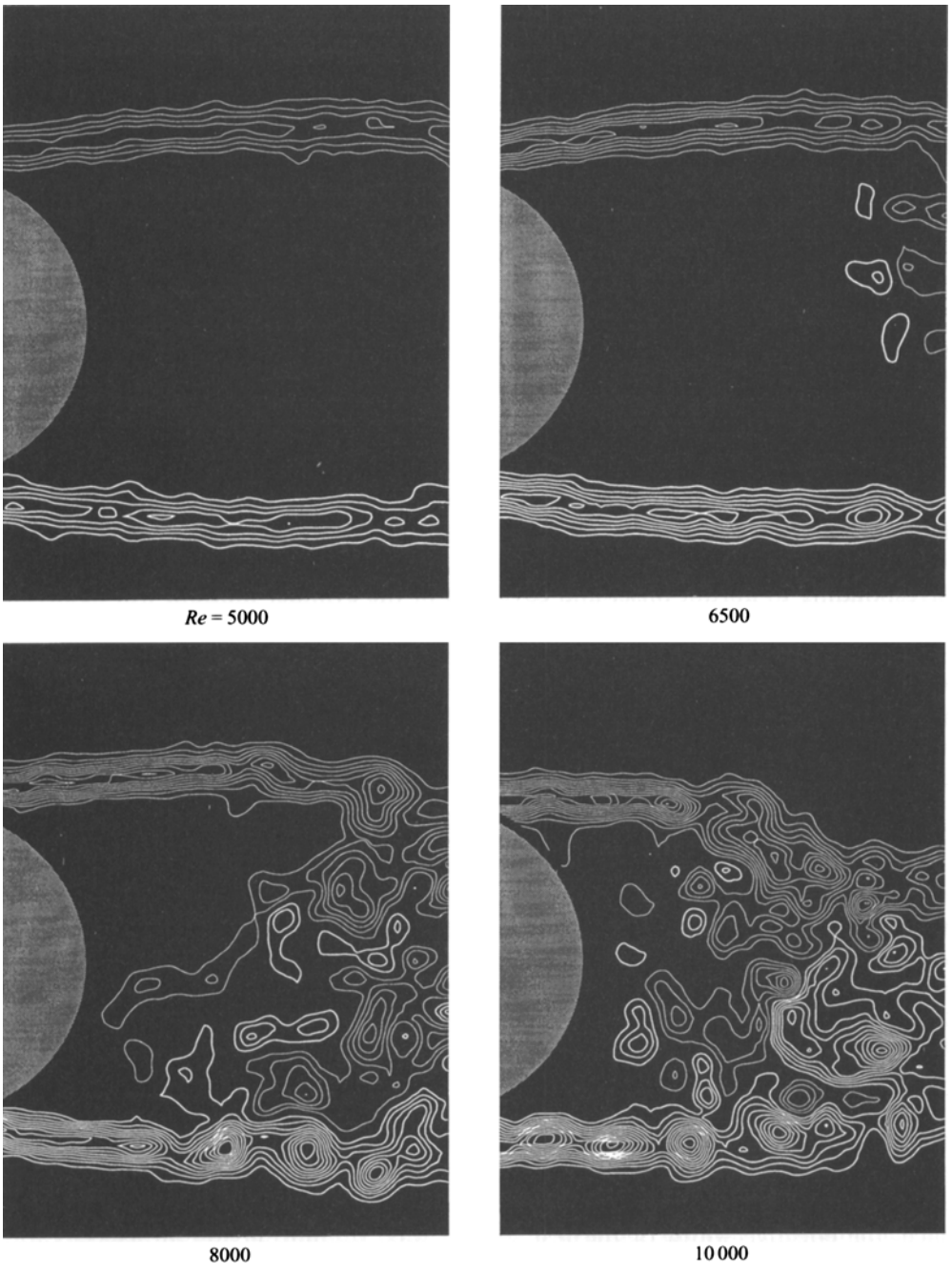

FIGURE 2. Instantaneous near-wake vorticity fields for a stationary cylinder over the range $5000 \leqslant Re \leqslant 10000$. Minimum contour level $|\omega_{min}| = 5\ s^{-1}$, contour increment $\Delta\omega = 5\ s^{-1}$. Positive contours: thin lines; negative contours: thick lines.

concentrations (Chyu & Rockwell 1996) than in the present facility, for which special efforts were made to minimize spectral contributions of the same order as f_i.

The motion of the cylinder was controlled by a high-resolution motor interfaced with a computer and attached to a traverse table. This system allowed controlled

perturbations of the cylinder in a direction perpendicular to the free stream at amplitudes $0.001 \leqslant A/D \leqslant 0.06$, corresponding to root-mean-square (r.m.s.) amplitudes $0.0007 \leqslant A_{rms}/D \leqslant 0.042$, and frequencies over the range $0.3 \leqslant f_e \leqslant 2.4$ Hz. The r.m.s. velocity v_e of forcing relative to the free-stream velocity U is $v_e/U = 2\pi f_e A/\sqrt{2}U_0$. At the lowest amplitude $A/D = 0.001$ and $f_e = f_i = 2.4$ Hz, $v_e/U = 0.006$. The first phase of the experiments involved steady-state periodic motion of the cylinder, while the second phase incorporated abrupt onset and cessation of the periodic motion, in order to allow examination of the transient response of the near wake.

Quantitative flow visualization involved a laser-scanning version of high-image-density particle image velocimetry (PIV), described by Rockwell *et al.* (1992, 1993), and Rockwell & Lin (1993). A scanning laser sheet was generated by steering the beam from a continuous wavelength Argon-ion laser (4 W) to a rotating mirror having 72 facets. A scanning frequency of 626 c s^{-1} was employed. This scanning frequency, in conjunction with the velocity of the bias mirror located in front of the camera lens, allowed optimum spacing between particle images of approximately 160 μm, while biasing the entire pattern of particle images, in order to preclude difficulties associated with directional ambiguity and large dynamic range across the image. These images were generated by seeding the flow with 12 μm diameter hollow glass spheres coated with a thin layer of silver. Particle images were recorded using a Nikon F4 camera with a 105 mm lens, with high resolution (300 lines mm^{-1}) 35 mm film as the recording medium. The entire system comprising the camera, the bias mirror, and motion of the cylinder were synchronized using a central microcomputer in the laboratory.

The lens system provided a magnification factor $M = 1{:}2.9$, defined as the ratio of the length scale on the film negative to the length scale in the physical plane of the laser sheet. The 35 mm negatives were digitized using a 35 mm film scanner at a scanning resolution of 125 pixels mm^{-1}. The digitized images were then evaluated to obtain the velocity vectors. An interrogation window size of 100 pixels × 100 pixels (0.8 mm × 0.8 mm) with 50% overlap was used, which resulted in a grid size of 0.4 mm × 0.4 mm on the film, corresponding to a grid of 1.2 mm × 1.2 mm in the plane of the laser sheet. Each interrogation square contained approximately 20–25 particle images. Evaluation of this pattern of images yielded one velocity vector by use of a single-frame cross-correlation approach.

Three quantitative representations of the flow field are employed. Velocity fields involve velocity vectors obtained directly from evaluation of the negative. Streamlines were determined with an algorithm that connected tangents to the instantaneous velocity vectors. Vorticity was calculated using an elemental circulation technique and is presented as contours of constant positive and negative vorticity.

The value of characterizing the Kármán vortex formation from a stationary cylinder on the basis of vorticity distributions at very low Reynolds numbers (up to $Re = 200$) was clearly demonstrated by Green & Gerrard (1993) using an analogous approach to PIV, namely direct particle tracking velocimetry (PTV). Further interpretation of their results is given by Griffin (1995), who focused on possible interpretations of the vortex formation length. The present study also includes consideration of the vortex formation length, but the general emphasis is on the instantaneous structure of both large and small scales at relatively high Re, and the manner in which they are altered due to perturbations of the cylinder. Sufficiently high spatial resolution is required; it is attained by appropriate design of the PIV-based system.

3. Structure of the wake from a stationary cylinder

Figure 2 shows representative contours of instantaneous positive (thin lines) and negative (thick lines) vorticity in the near wake, spanning a range of Reynolds number. At $Re = 5000$, isolated concentrations of vorticity are barely detectable. At higher values of Reynolds number, indications of small-scale shear-layer vortices are clearly evident, first on the right-hand side of the image at $Re = 6500$, then considerably closer to the cylinder at $Re = 8000$ until, at $Re = 10000$, highly concentrated vortices are apparent immediately downstream of separation from the cylinder. At the largest values of Re, these small-scale concentrations are detectable within the clusters of vorticity that represent the first stage of formation of the Kármán vortices. Moreover, regions of positive and negative vorticity are generally interspersed among one another. This observation suggests cancellation of vorticity during Kármán vortex formation and development, which is addressed in the investigations of Gerrard (1966) and Bearman & Obasaju (1982). Finally, an important general observation in figure 2 is that the onset of the vorticity agglomerations associated with Kármán vortex formation is strongly influenced by the onset of small-scale concentrations in the separating shear layer. At the highest value of $Re = 10000$, Kármán vortices develop close to the base of the cylinder, in accord with the abrupt formation of the first shear-layer vortex immediately downstream of separation.

The detailed structure of the separated layers from the bottom surface of the cylinder at $Re = 5000$ and 10000 is shown in figure 3. For the contours of constant vorticity given in images (*a*) and (*e*), the minimum vorticity level is the same at $\omega_{min} = 5\ \mathrm{s}^{-1}$, whereas the incremental level $\Delta\omega = 2\ \mathrm{s}^{-1}$ in (*a*) and $5\ \mathrm{s}^{-1}$ in (*e*). In (*a*), the closed contours of vorticity representing vorticity extrema are designated by the black arrows. These closed contours are confined to the innermost region of the vorticity layer. The wavelength λ between their centres is $0.43D$, and the average dimensionless circulation over one wavelength, associated with the second and third vorticity extrema is $\Gamma_\lambda = \Gamma/\pi U\lambda = 0.45$. On the other hand, at the higher value of Re represented in (*e*), the vorticity is highly concentrated, and the wavelength $\lambda = 0.23D$ between the vorticity concentrations designated by the arrows in the left half of the image; the average value of $\Gamma_\lambda = 0.42$ is, however, close to that of image (*a*).

The degree of concentration of vorticity ω is obtained by considering the first three peaks and valleys along the central portions of the vorticity contour patterns of images (*a*) and (*e*). The average maximum vorticity Ω_{max} was determined from a simple spatial average of the peak and valley values. The degree of vorticity concentration is expressed in normalized form as $c = \omega_{max}/\Omega_{max}$ where ω_{max} is the peak value of vorticity in each of the first three concentrations of vorticity. The values are $c = \omega_{max}/\Omega_{max} = 0.12$, 0.12 and 0.21 for the first, second and third concentrations in image (*a*); correspondingly, $c = 0.22$, 0.50 and 0.57 in image (*e*). The relatively high value of instantaneous vorticity concentration $c = 0.57$, associated with the third concentration in (*e*) is at a location just downstream of the base of the cylinder, $x/D = 0.55$, where x is measured from the centre of the cylinder. At approximately this same location, however, $c = 0.12$ in (*a*). We therefore conclude that, in the initial region of development of the separated layer, the normalized concentration of vorticity is nearly a factor of 5 higher at $Re = 10000$ than at $Re = 5000$.

These high values of vorticity concentration c in image (*e*) will be associated with relatively large fluctuations of vorticity and velocity as the train of vorticity concentrations translates past a given point of observation in the shear layer, and it is expected that the values of Reynolds stress will be substantially higher for the initial

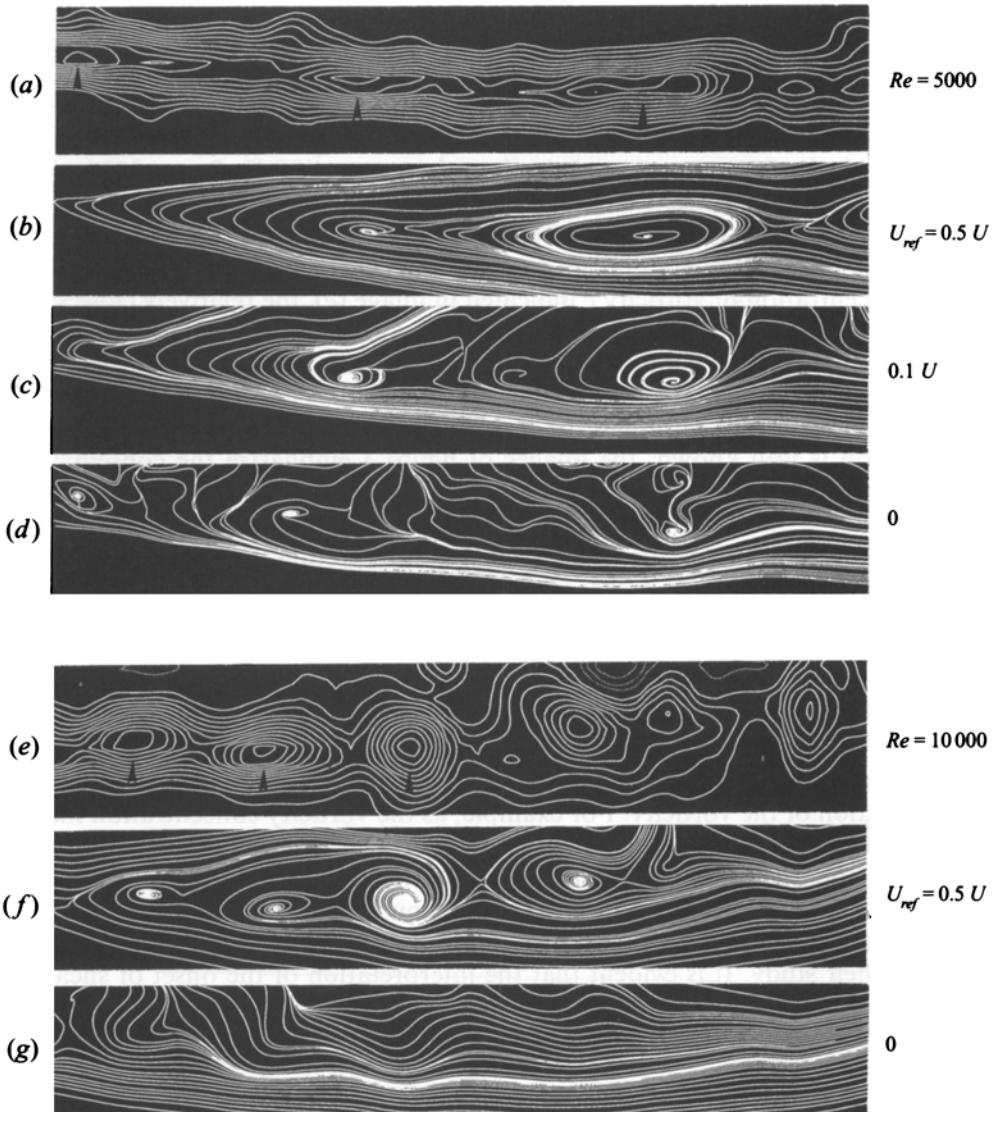

FIGURE 3. Closeups of instantaneous vorticity contours (*a*, *e*) and streamlines for the shear layer from the bottom surface of the cylinder at $Re = 5000$ (*a–d*) and $Re = 10000$ (*e–g*). Minimum vorticity contour level $\omega_{min} = 5\ s^{-1}$ in (*a*) and (*e*); increment $\Delta\omega = 2\ s^{-1}$ in (*a*) and $5\ s^{-1}$ in (*e*). For streamline patterns, U_{ref} is the velocity of the reference frame of observation. The free-stream velocity is U.

region of the layer at $Re = 10000$. The instantaneous value of $u'v'/U^2$ was evaluated at the location of the second extremum (peak) of vorticity in images (*a*) and (*e*). Its values were 0.00096 and 0.004 respectively. The larger value at $Re = 10000$ suggests a large increase in time-averaged turbulent shear stress. The consequence is an increased entrainment demand of the shear layer at $Re = 10000$, in turn decreasing the formation length of the first Kármán vortex, as shown in figure 2.

Corresponding streamlines are shown in various reference frames in figure 3(*b–d*) at $Re = 5000$. The frame $U_{ref} = 0.5U$ shows the saddle point structure, corresponding to locations where the streamlines tend to intersect, between the second, third and fourth

vorticity concentrations. For $U_{ref} = 0.1U$ in image (*c*), the spiralling streamline pattern has foci (apparent centres) at approximately the same location as the foci of (*b*) and, in turn, the locations of the extrema of the vorticity concentrations in (*a*). In the laboratory frame $U_{ref} = 0$; however, the centres of the lower-level vorticity concentrations are less well-defined, although they are generally identifiable as being associated with the first, second, and third vorticity extrema. At $Re = 10000$, the foci of the spiral streamline patterns are readily identifiable in figure 3(*f*), representing the frame $U_{ref} = 0.5U$, but in (*g*), corresponding to the laboratory frame $U_{ref} = 0$, spiral patterns do not exist, and it is difficult to determine whether a 'vortex' exists. Despite the high concentration of vorticity *c* indicated in image (*e*), the relatively close spacing of the concentrations precludes identification of vortices in the laboratory frame in image (*g*). On the other hand, the existence of vortices is suggested in the frames $U_{ref} = 0.1U$ and 0 in images (*c*) and (*d*), even though the concentration of vorticity *c* has a much lower value. Although the sensitivity of streamline patterns to the frame of observation is well known, the images of figure 3 emphasize the consequence of degree of concentration of vorticity for essentially the same dimensionless circulation Γ_λ.

These observations underscore the difficulty in interpreting the existence or strength of small-scale vortices in the separated layer from the cylinder based solely on visualization techniques that indicate instantaneous streamlines, e.g. particle streak visualization. In the event that streakline visualization using local injection of marker is employed, another type of difficulty is encountered, as demonstrated by Gursul & Rockwell (1991). By considering Stuart's (1967) solution for a spatially periodic mixing layer, which allows arbitrary concentration of vorticity, they show that the area over which the visualization marker is distributed is actually inversely related to the degree of concentration of the vorticity. For example, as the vorticity concentration increases by a factor of 5, and the spatial extent of the vorticity is decreased accordingly, the width of the apparent vortex occupied by the marker actually increases by a factor of 3, when the marker is not introduced at a location of zero fluctuating vorticity. The extreme values of vorticity concentration addressed in figure 3 fall within the range covered in their study. It is evident that the interpretation of the onset of shear-layer vortices, as well as their degree of concentration and circulation is most appropriately based on instantaneous distributions of vorticity.

4. Structure of the wake from a perturbed cylinder

The foregoing section shows that, at sufficiently high Reynolds number $Re = 10000$, the near wake is characterized by the rapid onset of small-scale shear-layer vortices, which comprise the large-scale Kármán structures. Application of small-amplitude perturbations at a lower value of Reynolds number $Re = 5000$ is expected to alter the onset and development of highly concentrated shear-layer vortices and, in turn, the Kármán vortex formation. The objective therefore is to apply highly controlled disturbances at a single frequency, and determine the quantitative instantaneous response of the near wake.

4.1. *Overview*

The overall response of the near wake is represented in figure 4. The excitation frequency f_e of the cylinder is normalized by the frequency f_i of the inherent shear-layer instability and the oscillation amplitude A is normalized with respect to cylinder diameter D. Lines A, B, and C represent threshold values of excitation conditions that induce states of the near wake defined by the shaded regions.

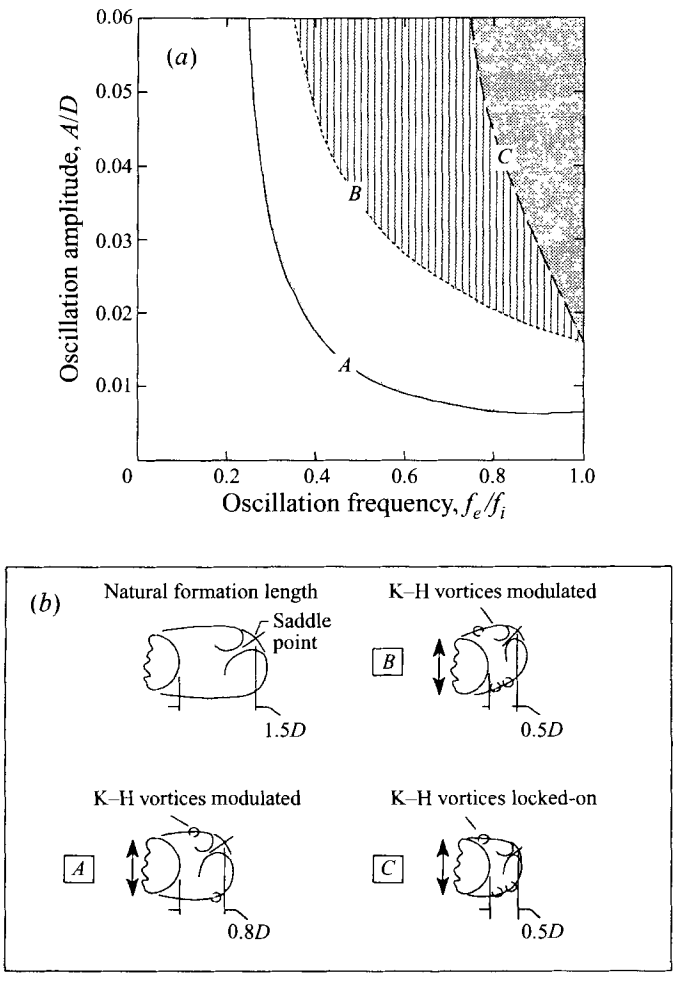

FIGURE 4. Regime map showing the response of the near wake to oscillation of the cylinder. f_e = oscillation frequency (Hz); f_i = frequency of inherent instability of separating shear layer. Ratio of shear layer to Kármán frequency is $f_i/f_K = 6.7$. $Re = 5000$.

The response diagram of figure 4 was obtained from extensive study of patterns of particle images of the near wake using a video system, as well as highly resolved quantitative interpretations of the near wake using the particle image velocimetry technique. The formation length of the Kármán vortices is defined by the saddle point indicated in each of the schematics at the bottom of figure 4. Line A represents the boundary for which substantial modification of the Kármán formation length, i.e. location of the saddle point, was attainable. It corresponds to a formation length of the large-scale Kármán vortices equivalent to that occurring for the self-excited wake at $Re = 10000$ (see figure 2). Above this line, for further increases of either amplitude A/D or frequency f_e/f_i, the Kármán formation length continues to decrease until a limiting state is reached. It is defined by line B and corresponds to a location of the saddle point approximately $0.5D$ downstream of the base of the cylinder. Moreover, for the entire domain of f_e/f_i *vs.* A/D lying below line C, the shear-layer vortices are not synchronized with the cylinder motion; rather, their locations drift up- and downstream. Line C, however, represents the threshold for phase-locked spatially

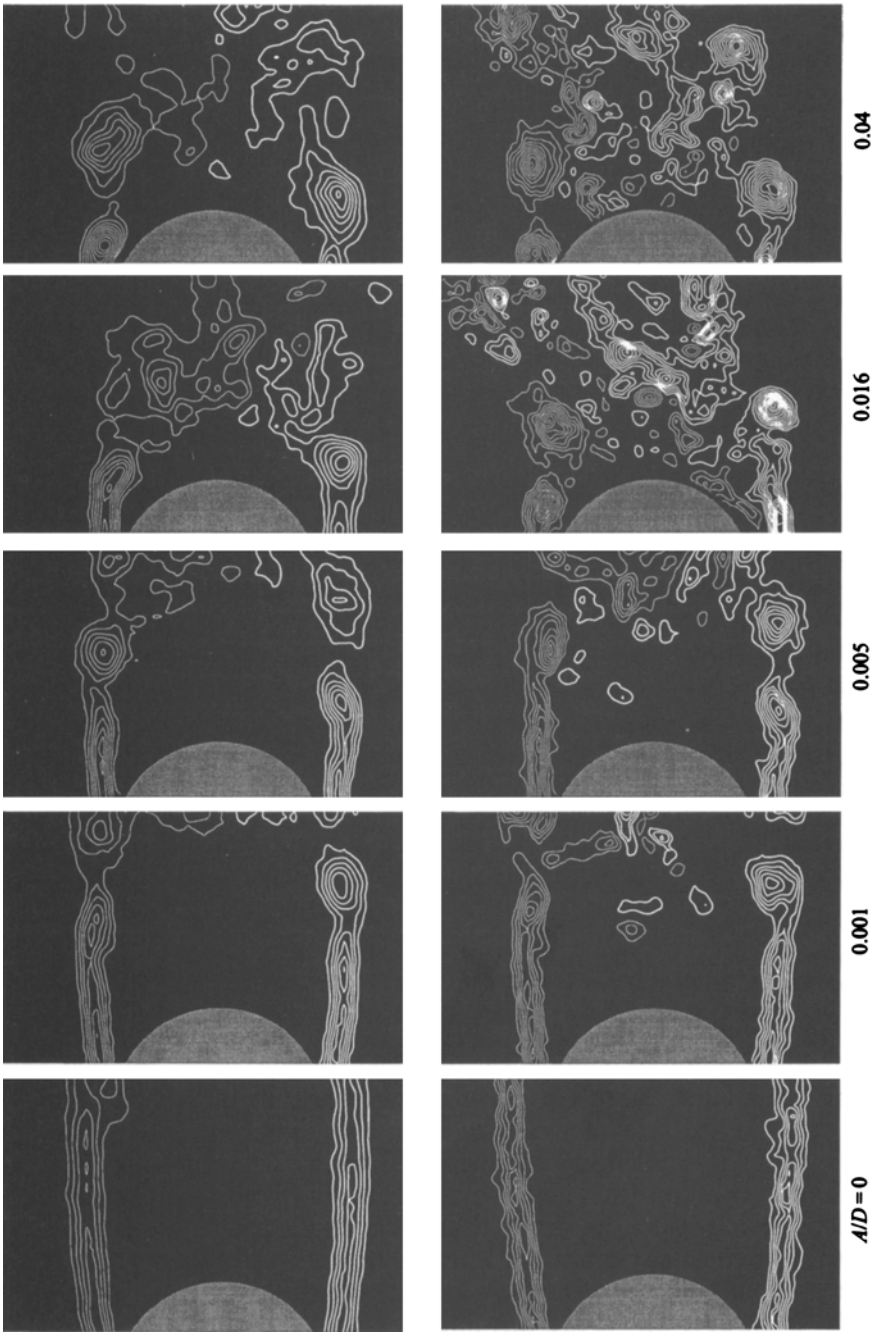

FIGURE 5(*a*). For caption see facing page.

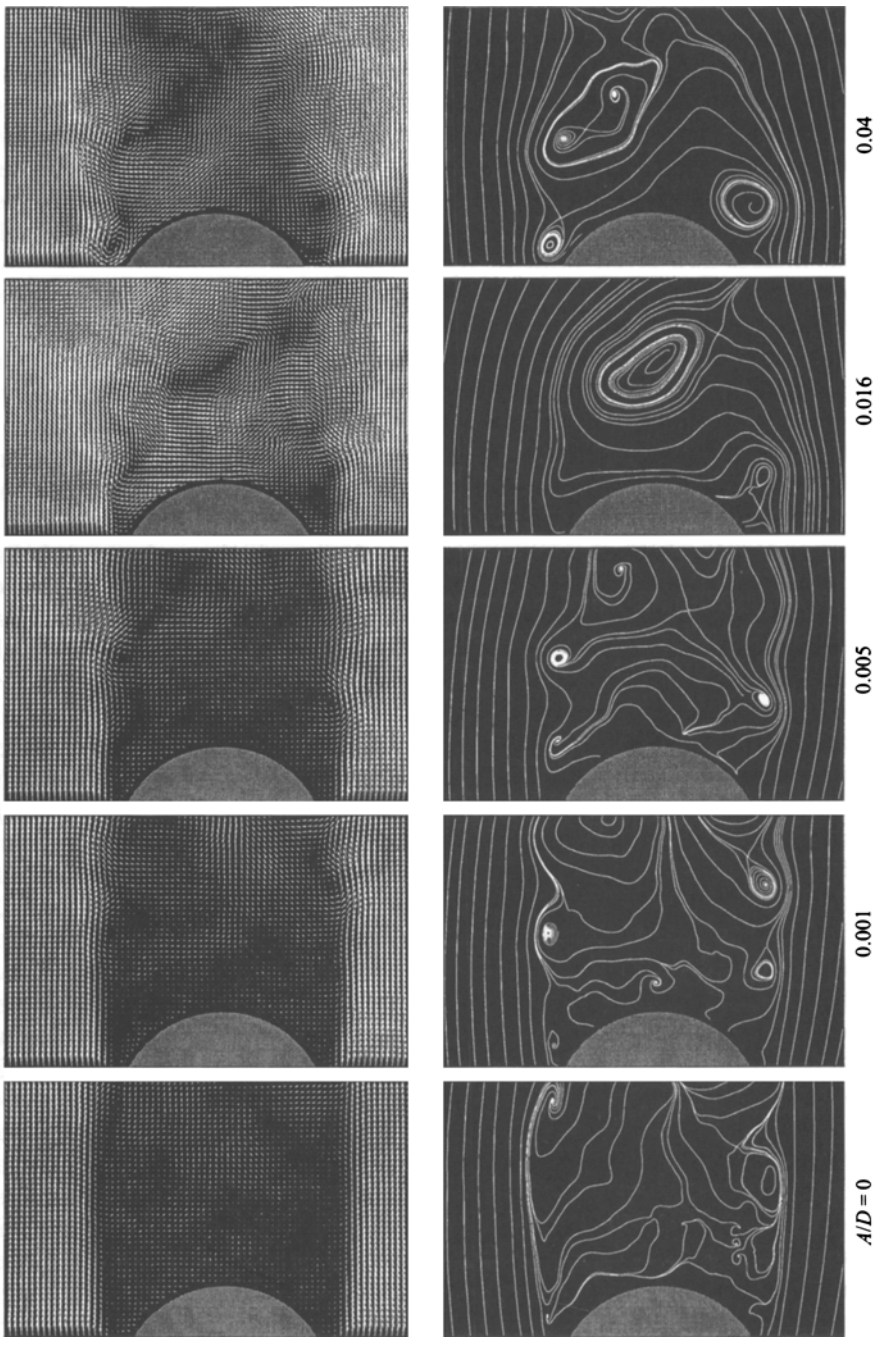

FIGURE 5. Excitation of cylinder at $f_e/f_i \simeq 1$, corresponding to $f_e/f_K \simeq 6.7$. (*a*) Top row: ensemble-averaged vorticity fields. Bottom row: instantaneous vorticity fields. Minimum contour level $|\omega_{min}| = 5\ s^{-1}$, contour increment $\Delta\omega = 5\ s^{-1}$. $Re \simeq 5000$. (*b*) Top row: ensemble-averaged velocity fields. Bottom row: averaged streamline patterns.

repetitive patterns of shear-layer vortices relative to the motion of the cylinder. In the following, the principal features of the near-wake response are clarified for each of the regimes shown in figure 4.

4.2. *Perturbation at instability frequency of shear layer: effect of amplitude on patterns of vorticity concentrations*

Figure 5(*a*) gives an overview of the amplitude response of the near wake for increasing A/D at $f_e/f_i = 1$. All images were acquired at the maximum positive displacement of the cylinder. Each image in the top row, showing contours of constant positive (white) and negative (grey) vorticity, is an ensemble- (phase) average of five successive instantaneous images. In the bottom row, corresponding instantaneous images are illustrated. It is evident that there is strong correspondence between the averaged and instantaneous images at a given value of A/D. The general location and form of the vorticity concentrations are generally similar, except at $A/D = 0.016$, where sequential images covering a number of cycles of excitation show substantial modulations of both the shear-layer and Kármán vortex systems, corresponding to significant changes in the instantaneous images from cycle to cycle. This modulation therefore yields an averaged image significantly different from the instantaneous one. At sufficiently high $A/D = 0.04$, however, these modulations give way to locked-on shear-layer vortices from cycle to cycle and strong correspondence between averaged and instantaneous images.

The formation length of the shear-layer vortices is strongly dependent on A/D. For the case of no excitation, i.e. $A/D = 0$, regions of highly concentrated vorticity are not detectable within the field of view, consistent with the images of figures 2 and 3. For the smallest-amplitude perturbation, $A/D = 0.001$, however, pronounced Kelvin-Helmholtz (K–H) concentrations are evident in both the ensemble-averaged and instantaneous images, and the initially formed vortex from the lower surface of the cylinder is at a distance $x_v/D = 1.10$, measured from the centre of the cylinder. It moves well upstream when the amplitude is increased to $A/D = 0.005$, and, at the largest amplitudes, $A/D = 0.016$ and 0.04, the first concentrated vortex is formed from the upper, rather than the lower, surface of the cylinder. If we focus on the formation length L_f of the first highly concentrated vortex in the ensemble-averaged layer from the lower surface of the cylinder, shown in the upper row of images of figure 5*a*, it is evident that L_f decreases with increasing A/D until a saturation value close to the base of the cylinder, corresponding to $x_v/D = 0.57$, is attained at $A/D = 0.016$; this value is maintained at $A/D = 0.04$. The circulation of the initially formed vortex, expressed in dimensionless form as $\Gamma^* = \Gamma/2\pi UD$, is essentially constant with values $0.18 \leqslant \Gamma^* \leqslant 0.20$ for amplitudes up to $A/D = 0.016$, then increases to $\Gamma^* = 0.29$ at $A/D = 0.04$.

The foregoing observations indicate the coincidence of several events at the threshold amplitude $A/D = 0.016$: (*a*) attainment of a limiting value of formation length of the first highly concentrated vortex in the shear layer, (*b*) an increase in circulation of this vortex (at $A/D = 0.004$); (*c*) a change in timing of the first highly concentrated shear-layer vortex relative to the cylinder motion; and (*d*) as suggested by the lack of close correspondence between the instantaneous and averaged images at $A/D = 0.016$, onset of a modulated K–H vortex pattern, which returns to a phase-locked pattern at $A/D = 0.04$. This aspect will be addressed in detail in figures 6 and 7.

These events in the shear layers have important consequences in the region between the shear layers. Clusters of positive (thick lines) and negative (thin lines) vorticity

move progressively upstream as A/D is increased. This upstream migration of vorticity is particularly evident in the instantaneous images. For the case of the unperturbed cylinder ($A/D = 0$), no detectable vorticity is evident in this region between the shear layers; it is first indicated at $A/D = 0.001$. At $A/D = 0.016$, the clusters of instantaneous positive and negative vorticity in the central region of the wake appear adjacent to the base of the cylinder. This effect is apparently associated with an increased entrainment demand of the shear layers, imposed by increased Reynolds stresses arising from earlier formation of shear-layer vortices with highly concentrated vorticity. It is equivalent to the effect observed with increasing Reynolds number (for the unperturbed cylinder), as addressed in figures 2 and 3. Indeed, a large increase in instantaneous Reynolds stress is associated with the increase in degree of concentration of vorticity, as described in §3.

4.3. *Perturbation at instability frequency of shear layer: effect of amplitude on topology*

Distributions of averaged velocity and streamline patterns are shown in figure 5(*b*). At $A/D = 0$ and 0.001, the velocities in the base region are indeed small. The velocity magnitudes in the base region increase dramatically, however, at higher values of A/D, and at $A/D = 0.0016$ and 0.04, the entire region of the near wake immediately adjacent to the base of the cylinder participates in the formation of the shear-layer vortices and most likely the large-scale Kármán vortices as well. These observations can be interpreted more quantitatively by describing the topology of the corresponding streamlines.

The streamline topologies of figure 5(*b*) correspond to the small-scale concentrations of vorticity, i.e. shear-layer vortices, of figure 5(*a*). Patterns of spiralling streamlines are evident in the shear layers separating from the cylinder for all amplitudes A/D. These spiral patterns are in contrast to the nested pattern of concentric closed streamlines that represents purely two-dimensional shear-layer vortices (Perry, Chong & Lim 1982). An inward spiral corresponds to a stable focus and stretching of the vortex along its span; conversely, an outward spiral defines an unstable focus and spanwise contraction. At the smallest values of A/D, $0 \leqslant A/D \leqslant 0.005$, the small-scale spirals are predominantly inward, indicating stable foci. At the largest values of $A/D = 0.016$ and 0.04, the first pronounced vortex forms immediately downstream of the cylinder (lower side, $A/D = 0.016$; upper side, $A/D = 0.04$) and the topology exhibits a well-defined limit cycle adjacent to a saddle point, defined by the point of intersection of intersecting streamlines. Also, in the region immediately adjacent to the base of the cylinder, several streamlines extend across the entire wake, thereby linking topological features on opposite sides of the wake.

The onset and development of large-scale vortical structures in the near wake generates topological patterns that are linked to those of smaller-scale vortices described in the foregoing. At the smallest values of $A/D = 0$ and 0.001, the pattern of streamlines in the central portion of the wake indicates no large-scale vortical activity within the field of view; instead, the streamline patterns along the central portion of the wake, which are oriented in the upstream direction, systematically diverge and connect to the shear layers separating from the cylinder. In essence, this pattern is induced by the entrainment demands of the shear layers, arising from the small-scale spiral patterns induced by excitation of the cylinder. At larger values of $A/D \geqslant 0.005$, a larger-scale swirl pattern of streamlines appears in each of the images; its centre (focus) is approximately $0.6D$ to $1.0D$ downstream of the base of the cylinder, and it is located in the upper half of the wake. Correspondingly, a saddle point appears

beneath the larger-scale spiral pattern at $A/D = 0.005$. With increasing A/D, it rotates counterclockwise towards the upper shear layer until, at $A/D = 0.04$, it is above the plane of symmetry of the wake. This rotation of the saddle point corresponds to earlier formation and increased circulation of the shear-layer vortices.

The topology of the larger-scale vortical structures at the values of $A/D = 0.016$ and 0.04 shows well-defined limit cycles immediately within the intersecting streamlines that form the saddle point. Within the limit cycle at $A/D = 0.016$, another nested limit cycle is evident; it suggests a single larger-scale concentration of vorticity and corresponds to the broadly distributed vorticity shown in the averaged image of figure 5(*a*). The limit cycle at $A/D = 0.04$ contains two smaller-scale foci, corresponding to the two primary clusters of vorticity in the corresponding averaged image of figure 5(*a*).

Although these topological features at large A/D suggest the occurrence of Kármán vortices close to the base of the cylinder, this observation is not conclusive. The occurrence of shear-layer vortices having relatively high values of circulation, especially at $A/D = 0.016$ and 0.04, distorts the streamline patterns. A spatial filtering technique is required to extract the largest-scale features of the near wake associated with the Kármán vortex formation at successive instants during the Kármán cycle; the next sub section focuses on this aspect.

4.4. *Perturbation at instability frequency of shear-layer: consequence for Kármán vortices*

In order to determine the inter-relationship between the forced shear-layer vortices and the naturally occurring Kármán vortices, cases of relatively large-amplitude excitation were considered as shown in figures 6 and 7. They correspond respectively to regimes *B* and *C* of figure 4.

For the case of the amplitude $A/D = 0.016$, shown in figure 6, a long time sequence of images was considered. Each image in the sequence corresponds to triggering the camera at the maximum-positive displacement of each cycle having a period equal to that of the shear-layer instability. The three sets of images selected for figure 6 represent the minimum to convey the central message. These images are spaced at three cycles, designated as $N = 1$, 4 and 7. This spacing was chosen because approximately six complete cycles corresponds to one complete Kármán cycle. Considering first the instantaneous contours of constant vorticity shown in the top row of images of figure 6, it is evident that the initially formed concentrations of vorticity from the top and bottom surfaces of the cylinder are of a generally similar form and at nearly the same location for $N = 1$ and 7. In contrast, the pattern of initially formed vortices in the image at $N = 4$ is approximately a mirror image of those at $N = 1$ and 7. This sequence, representative of a large number of successive images, shows that the pattern of initially formed shear-layer vortices is modulated such that it repeats approximately every six cycles, i.e. every Kármán cycle. The overall pattern of the vorticity distributions is oriented downward at $N = 1$ and 7, and upward at $N = 4$.

In order to determine the possible relationship between the Kármán vortex formation and the observed undulations of the wake shown in the top row of images of figure 6, the instantaneous velocity fields were low-pass filtered such that length scales smaller than $0.76D$ were eliminated, as shown in the middle row of figure 6. The consequence of this filtering is therefore to eliminate the small-scale vortices in the shear layer and to highlight the large-scale (Kármán) vortex formation. A large-scale swirl pattern of velocity vectors is suggested in each of these filtered velocity images by the pinwheel-like fringes surrounding each black hole, i.e. region of essentially zero

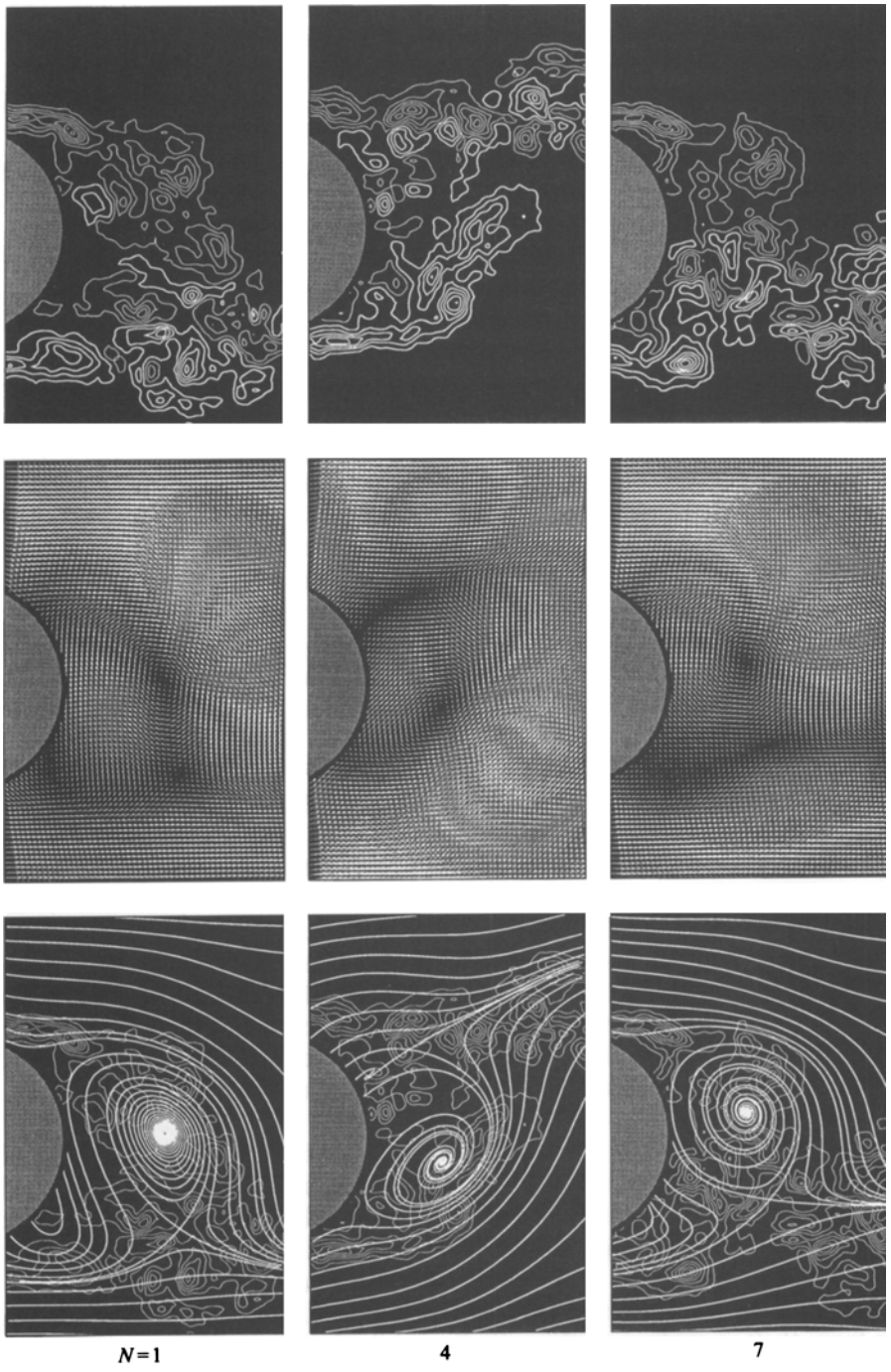

FIGURE 6. Excitation of cylinder at $f_e/f_i = 1$, corresponding to $f_e/f_K = 6.7$, and $A/D = 0.016$. Top row: instantaneous vorticity fields, minimum contour level $|\omega_{min}| = 5\ s^{-1}$, contour increment $\Delta\omega = 10\ s^{-1}$. Middle row: filtered velocity fields. Bottom row: vorticity fields with corresponding filtered streamline patterns. $Re = 5000$.

velocity. These black regions correspond to the centres, or foci, of the large-scale Kármán vortices. A Kármán vortex appears to form from the upper surface of the cylinder in images $N = 1$ and 7, while a corresponding vortex forms from the lower surface at $N = 4$. Streamline patterns corresponding to the filtered velocity fields are superposed on the unfiltered vorticity contours in the bottom row of images of figure 6. These patterns are very similar at $N = 1$ and 7: a saddle point occurs at the bottom of the near wake, and the streamline pattern indicating the vortex spirals outwards (evident from magnification of the pattern of velocity vectors). This outward spiral represents an unstable focus, defined in conjunction with figure 4(*b*). A nearly mirror-image pattern occurs at $N = 4$. An important conclusion therefore is that the modulated vorticity concentrations arising from excitation at the frequency of the shear layer take on patterns that are coupled with formation of the large-scale Kármán vortices. The wake undulates, i.e. 'swings' up and down, at the Kármán frequency. The amplitude of this wake swing is far in excess of what one would expect to occur at this very small amplitude of the cylinder perturbation. It appears that these particular patterns of shear-layer vortices, which are non-phase-locked at the excitation frequency, but spatially repetitive at the Kármán frequency, serve to amplify the transverse excursions, or swinging motion, of the entire near wake at the Kármán frequency. In other words, the modulated interaction of the shear-layer vortices represents a type of resonant effect that leads to highly amplified global motion of the wake. Considering the map of figure 4, this global response occurred primarily at larger values of A/D in regime B, while low values of A/D in regime B, modulated formation of the shear-layer vortices persisted, with less significant undulations of the entire near wake.

On the other hand, at a higher value of amplitude $A/D = 0.04$, represented by the images of figure 7, phase-locked patterns of shear-layer vortices were attained in the near wake; such patterns correspond to regime C in figure 4. In this case, no modulation of the type shown in figure 6 was present; therefore images corresponding to three successive cycles of excitation, $N = 1$, 2 and 3, i.e. approximately one-half Kármán cycle, are shown. The top row of images showing contours of constant vorticity indicates that the first two negative (thin lines) shear-layer vortices from the upper surface of the cylinder appear at approximately the same location in each image; similarly, the first two vortical structures from the bottom surface of the cylinder generally show a similar consistency. The basic features of this type of phase-locking of the initially formed vortices in the shear layer were first addressed in the preliminary study of Chyu *et al.* (1995).

The instantaneous velocity fields corresponding to the vorticity contours of the top row of images of figure 7 were filtered in the same manner as for figure 6. These filtered velocity fields, shown in the middle row of images, can be interpreted in the same spirit as the corresponding ones of figure 6. A Kármán vortex from the bottom surface of the cylinder is evident at $N = 1$. At $N = 2$, this vortex has moved downstream, and a smaller one has formed near the top surface. Finally, at $N = 3$, a large-scale vortex now appears from the top surface of the cylinder, while that from the bottom surface is no longer evident.

The streamlines centred on the Kármán vortices exhibit an inward spiral, i.e. stable focus at $N = 1$ and 3, in contrast to the consistently unstable focus observed for the modulated case of figure 6. On the other hand, during the transformation from the state at $N = 1$ to that at 3 in figure 7, unstable foci occur at $N = 2$.

The instantaneous streamline patterns corresponding to these filtered instantaneous velocity fields were originally assessed by Chyu *et al.* (1995). They are shown in the

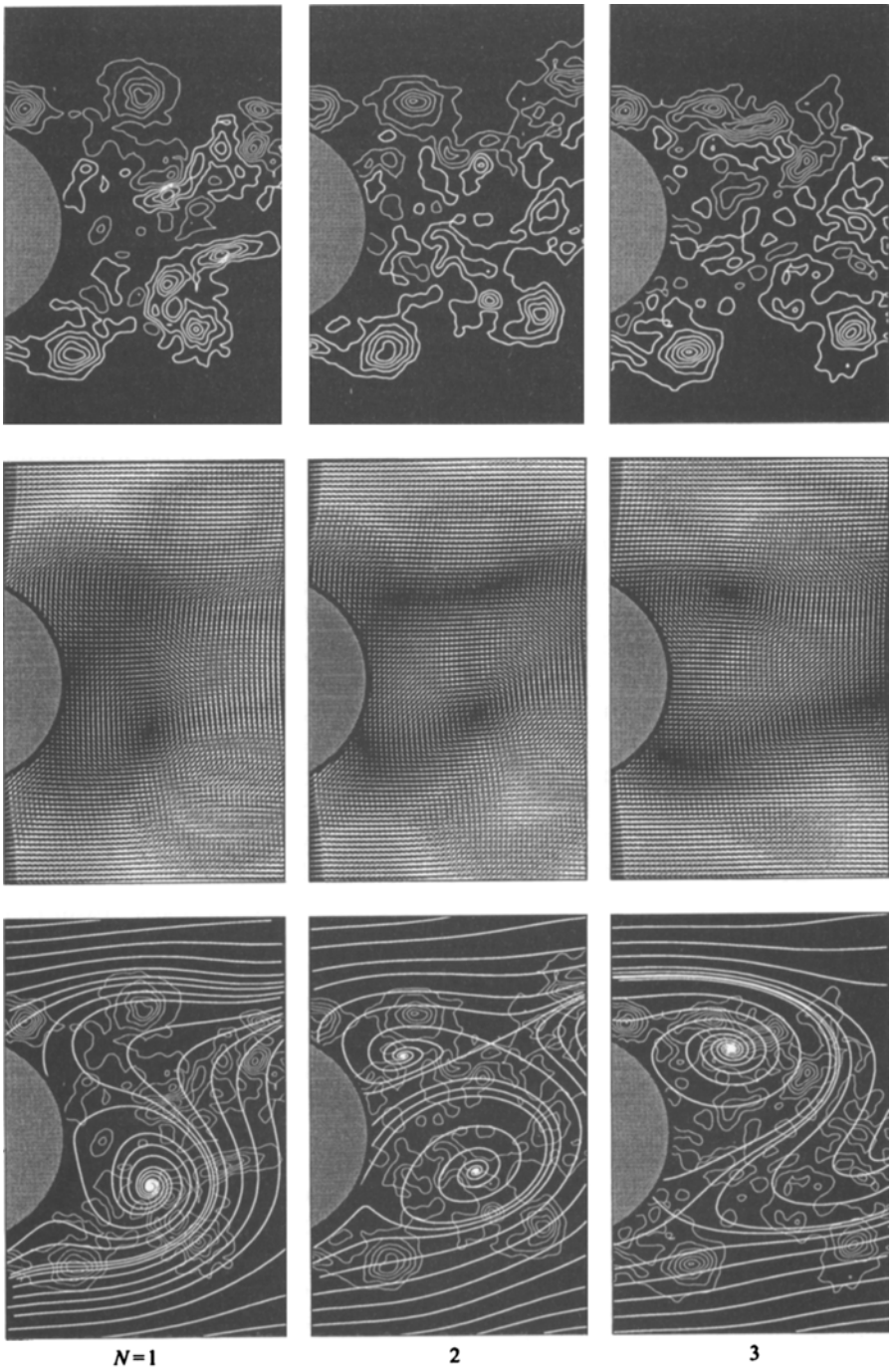

FIGURE 7. Excitation of cylinder at $f_e/f_i = 1$, corresponding to $f_e/f_K = 6.7$, and $A/D = 0.04$. Top row: instantaneous vorticity fields, minimum contour level $|\omega_{min}| = 5\ s^{-1}$, contour increment $\Delta\omega = 10\ s^{-1}$ (from Chyu *et al.* 1995). Middle row: filtered velocity fields. Bottom row: vorticity fields with corresponding filtered streamline patterns (from Chyu *et al.* 1995). $Re = 5000$.

bottom row of figure 7. In accord with the filtered velocity fields, the streamline topology indicates large-scale vortex formation from the bottom surface of the cylinder at $N = 1$. It progresses to the right at $N = 2$ and is no longer evident at $N = 3$. On the other hand, the initial stages of large-scale vortex formation from the upper surface of the cylinder are suggested by the topology at $N = 2$, and its further development at $N = 3$. The types of spiral streamline patterns, foci, and saddle points shown in figure 7 are what one expects for a self-excited wake at much higher Reynolds number, for which natural vortex formation occurs close to the base of the cylinder.

The interesting conclusion drawn from the observations of figure 7 is that first a locked-on, or phase-locked, pattern of shear-layer vortices can be generated in the near wake of the cylinder. This phase-locked pattern can then coexist with the spatial and temporal evolution of the large-scale Kármán vortex formation in the near-wake region (Chyu *et al.* 1995). These cyclic-repetitive phase-locked patterns of shear-layer vortices do not allow the large-scale transverse undulations or 'swinging' of the entire near wake at the Kármán frequency, as is the case for regime *B* represented by figure 6.

4.5. *Perturbation at subharmonics of instability frequency of shear layer*

Substantial modification of the near-wake structure is attainable at not only the most unstable frequency f_i of the shear layer separating from the cylinder but also its subharmonics (see figure 4). Cases of excitation at $f_e/f_i = \frac{1}{4}$, $\frac{1}{3}$ and $\frac{1}{2}$ are given in figure 8. For each of these cases of subharmonic excitation, A/D was adjusted in order to maintain the product $f_e A$ constant. As a reference case, consider the vorticity layers from the stationary cylinder, corresponding to $A/D = 0$, shown in figure 5(*a*). No concentrations of vorticity are evident within the field of view. On the other hand, the top row of images in figure 8, showing averaged distributions of vorticity, all indicate clusters of vorticity in the field of view for frequency ratios $f_e/f_i = \frac{1}{4}$, $\frac{1}{3}$ and $\frac{1}{2}$. The corresponding patterns of averaged velocity in the middle row of figure 8 exhibit swirls that occur closer to the base of the cylinder with increasing frequency ratio f_e/f_i. The instantaneous structure of the near wake is represented by the instantaneous contours of positive and negative vorticity in the bottom row of figure 8. At $f_e/f_i = \frac{1}{4}$, regions of positive and negative vorticity occur in the base region between the separating shear layers. At a higher value of $f_e/f_i = \frac{1}{3}$, the upper shear layer curls into a large-scale vortex, and at $f_e/f_i = \frac{1}{2}$, a similar curling back of the upper shear layer occurs, but its extent and complexity are more pronounced, with naturally occurring vortices evident along the entire extent of the shear layer.

The agglomeration of small-scale vorticity concentrations to form large-scale vortices close to the base of the cylinder might be expected to have analogies with the simpler configuration of an isolated mixing layer, such as that from a sharp-edged splitter plate. It is well known that the phenomenon of 'collective coalescence' can occur in a mixing layer when subharmonic perturbations are applied (Ho & Huang 1982). Provided the amplitude of the perturbation is sufficiently large, there is an abrupt simultaneous coalescence of small-scale vortices arising from the inherent instability of the mixing layer. Collective coalescence, in the traditional sense, does not appear to be attainable in the separated layers of the near wake, at least for the range of parameters considered herein. It is important to distinguish between the isolated mixing layer and the present system of two separated (mixing) layers with a base flow between them. These separated layers eventually comprise the large-scale vortices, which in turn modify the very near-wake region. This distinguishing feature gives rise to upstream movement of the vorticity concentrations in the central portion of the

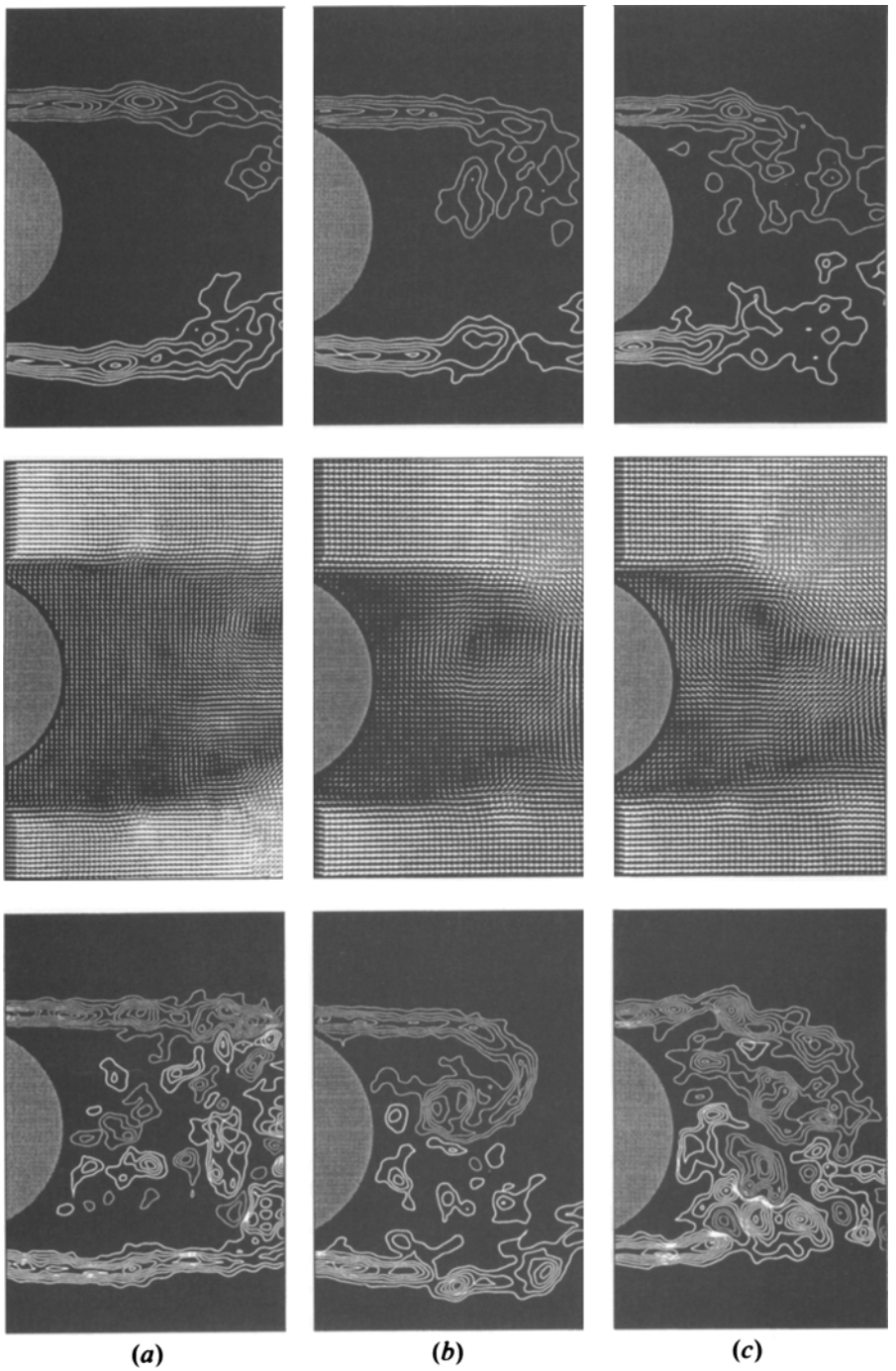

FIGURE 8. Excitation of cylinder at subharmonics of the inherent instability frequency (f_i) of the shear layer. First subharmonic corresponds to $f_e/f_i = \frac{1}{2}$ and $f_e/f_K = 3.35$. Top row and middle row: averaged vorticity and velocity fields. Bottom row: instantaneous vorticity fields. $|\omega_{min}| = 5\ \mathrm{s}^{-1}$, $\Delta\omega = 5\ \mathrm{s}^{-1}$. (*a*) $f_e/f_i = \frac{1}{4}$, $A/D = 0.04$; (*b*) $f_e/f_i = \frac{1}{3}$, $A/D = 0.03$; (*c*) $f_e/f_i = \frac{1}{2}$, $A/D = 0.02$. $Re = 5000$.

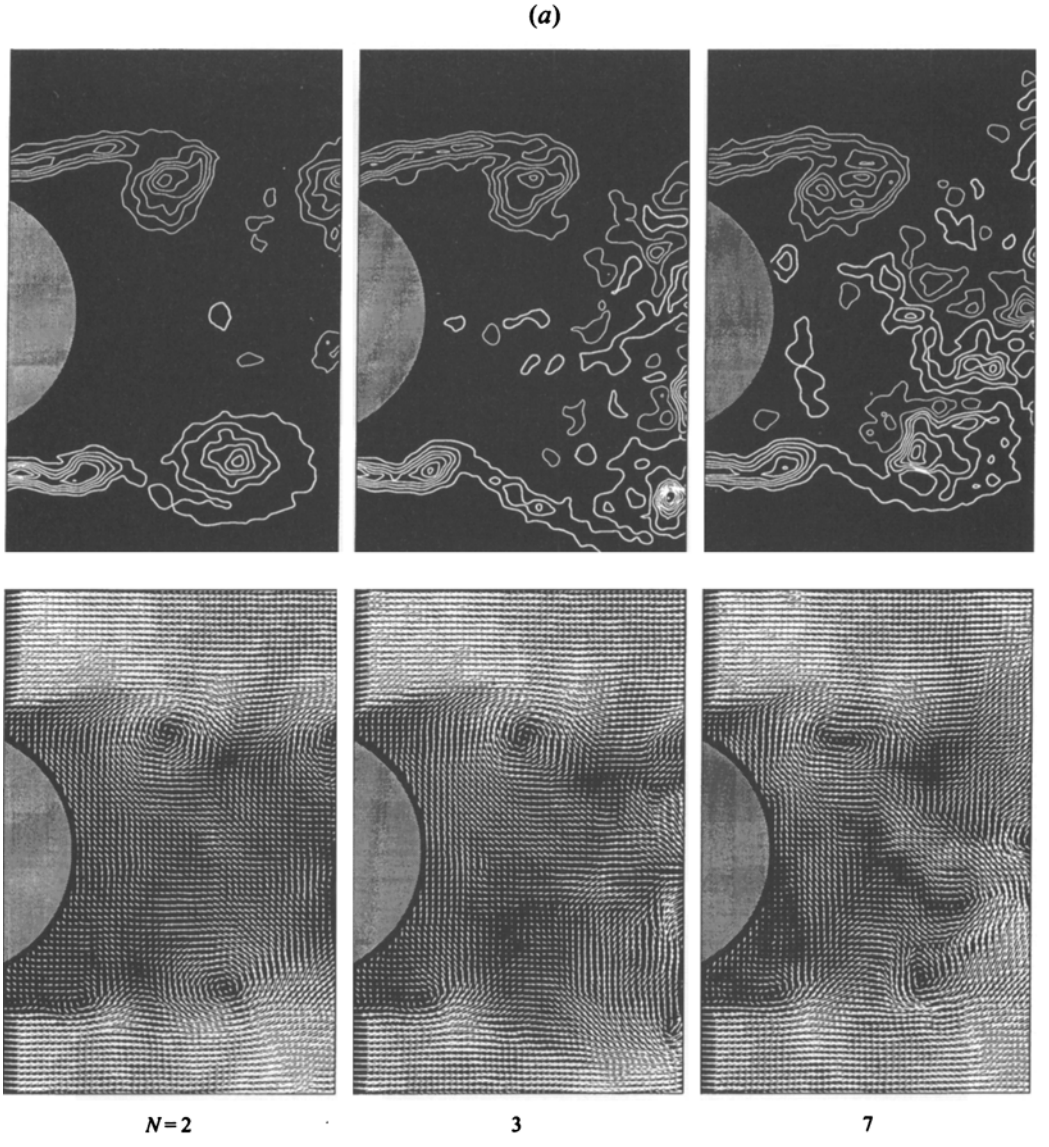

FIGURE 9(*a*). For caption see facing page.

wake, evident in the instantaneous image of figure 8(*a*) corresponding to $f_e/f_i = \frac{1}{4}$, as well as curling up of the upper shear layer, evident in the instantaneous image of figure 8(*b*) representing $f_e/f_i = \frac{1}{3}$. A similar curling up of the separated layer occurs in the instantaneous image of figure 8(*c*) corresponding to $f_e/f_i = \frac{1}{2}$; in induces agglomeration of as many as six vortices in the shear layer, but in a distinctly different fashion than for collective coalescence in an isolated mixing layer.

It is evident from both the averaged and instantaneous images at $f_e/f_i = \frac{1}{2}$ that simple subharmonic excitation draws the entire pattern of vortical structures close to the base of the cylinder. This pattern alternates from cycle to cycle and persists in this fashion during the steady-state periodic motion. In order to determine the possible states of the near wake leading to this type of structure, we consider its transient response, as described in the next sub section.

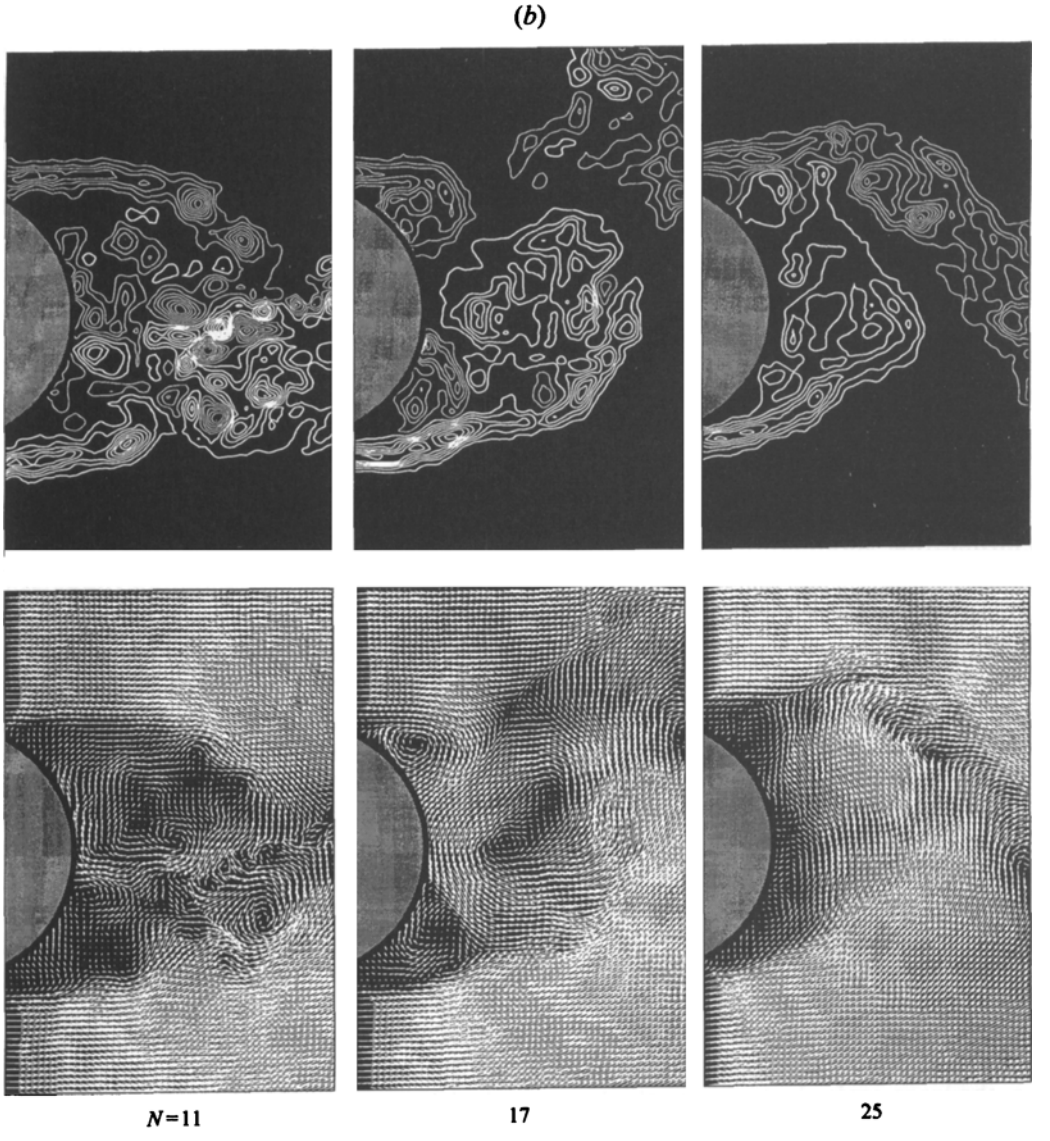

FIGURE 9. Transient response to onset of cylinder perturbation. Excitation is at $f_e/f_i = \frac{1}{2}$, corresponding to $f_e/f_K = 3.35$, and $A/D = 0.04$. Top row: instantaneous vorticity fields. Bottom row: instantaneous velocity fields. $|\omega_{min}| = 5\ s^{-1}$, $\Delta\omega = 7.5\ s^{-1}$. $Re = 5000$. (*a*) $N = 2$, 3 and 7; (*b*) $N = 11$, 17 and 25.

4.6. *Transient response to onset of perturbation: contraction of near wake*

For the initial state of the unperturbed wake shown in figure 5(*a*) ($A/D = 0$), the cylinder was subjected to applied perturbations at a frequency ratio $f_e/f_i = \frac{1}{2}$ and an amplitude $A/D = 0.04$. Let $N = 0$ represent the onset of the cylinder motion. The transient development of the near wake is represented by the images of figure 9(*a*), corresponding to cycles $N = 2$, 3 and 7 of the perturbation at one-half the inherent shear-layer frequency, i.e. $f_e = f_i/2$. All images correspond to the same instantaneous position of the cylinder, i.e. its maximum positive displacement. These images were

selected from the complete sequence in order to illustrate key features of the temporally and spatially developing wake.

Consider first the instantaneous distributions of vorticity in the top row of figure 9(*a*). It is evident that all three images show moderate-scale concentrations of vorticity in the upper shear layer, which have the same general form and location, i.e. they are phase-locked at the subharmonic excitation frequency. On the other hand, the form of the vorticity concentrations in the lower layer from the cylinder alternates between the states shown at $N = 2$ and 3. In other words, the lower layer exhibits one pattern of vorticity concentrations at $N = 2$ and 7, and another pattern at $N = 3$ and 8 (not shown). Detailed inspection of all images in this sequence shows that the largest clusters of vorticity in the top and bottom shear layers from the cylinder are formed from pairing of adjacent concentrations of small-scale vortices in the shear layer, while the smallest concentration in the bottom layer is not paired. The wavelength between the paired concentrations of vorticity in the upper layer is consistently $\lambda/D = 0.72$. In the lower layer, however, the spacing between the unpaired and paired concentrations of vorticity varies dramatically: in images $N = 2$ and 7, where the pattern is nearly repetitive, $\lambda/D = 0.62$ and 0.69 respectively; in image $N = 3$, however, $\lambda/D = 0.98$. During this modulation, the difference Δ in spacing between the first (paired) concentration of vorticity from the upper surface and the corresponding (unpaired) concentration from the lower surface is as follows: for $N = 2$ and 7, $\Delta/D = 0.32$ and 0.30; and for $N = 3$ and 8, $\Delta/D = 0.42$ and 0.37. This initial offset Δ of the first vortex from the top and bottom surfaces of the cylinder and its variation with N apparently serves as the initial condition for substantial modulations in wavelength between the paired and unpaired concentrations in the lower layer. These modulations are, in turn, related to the instantaneous circulation of the vortical structures. In the upper layer, this circulation $\Gamma^* = \Gamma/\pi UD$ has values in the range $0.28 \leqslant \Gamma^* \leqslant 0.33$. In the lower layer, the unpaired concentrations of vorticity have values of Γ^* over the range $0.15 \leqslant \Gamma^* \leqslant 0.16$. The paired concentrations in the lower layer at $N = 2$ and 7 have values $\Gamma^* = 0.43$ and 0.35. It is therefore evident that the paired concentrations in the lower layer can have a value of Γ^* somewhat larger than that of the paired concentrations in the upper layer. This difference in circulation is an additional feature of the modulated near wake.

Viewing all of the images of figure 9(*a*) together, one concludes that shortly after the onset of oscillation, the region near the base of the cylinder is essentially vorticity free, i.e. the large-scale clusters of vorticity concentrations in the central region of the wake at $N = 2$ and 3 are located well downstream. It is therefore possible for coalescence of adjacent small-scale vortices to occur in the same fashion as for an isolated mixing layer. The occurrence of the alternating paired–unpaired sequence in the lower layer, however, relative to the consistently paired sequence in the upper layer, suggests that coupling occurs between the shear layers separating from the cylinder; this effect is not present, of course, for the classical mixing layer.

The rhythmic variation of vortex patterns in images $N = 2$–7 gradually draws irregular clusters of vorticity upstream, through the central portion of the wake, to the base region. Owing to the increased Reynolds stress of the perturbed layers from the cylinder, their entrainment demands increase and the end effect is 'pumping' of fluid towards the base of the cylinder. This process continues until, at $N = 11$ in figure 9(*b*), the ordered patterns of vorticity concentrations formed from the cylinder collapse to simple layers of unpaired small-scale concentrations in the shear layer. These layers merge at the plane of symmetry of the base region. This intermediate state of the wake is followed by that at $N = 14$ (not shown), then that at $N = 17$. At $N = 14$, the anti-

symmetry of large-scale clusters becomes apparent; the upper shear layer curls back into the base region. Then, at $N = 17$, the large-scale cluster of positive (thick lines) vorticity from the bottom surface of the cylinder, which may be viewed as a Kármán-type vortex, induces a negative (thin lines) cluster from the base of the cylinder, arising from eruption of vorticity from the base. Simultaneously, the negative (thin lines) Kármán vortex from the upper surface of the cylinder undergoes its initial stage of formation. At $N = 25$, the limiting state is attained. The large-scale concentration of positive (thick lines) vorticity, again representing the Kármán vortex, is formed very close to, and extends along, the entire base. It deflects outward the developing shear layer from the upper shoulder of the cylinder. At larger values of N, i.e. longer times, the pattern of vortex formation persists in this form.

The circulation of the white, Kármán-type vortices at $N = 17$ is $\Gamma^* = 0.89$, which is more than five times the value of $\Gamma^* = 0.16$ for the unpaired shear-layer (K–H) vortex and over twice the $\Gamma^* = 0.39$ for the paired vortex in the lower layer of figure 9(*a*). This remarkable transformation in the structure of the wake from images $N = 2$–17 therefore yields a large increase in circulation of the initially formed vortices. The final limit-cycle structure of the initially formed Kármán vortex at $N = 25$ corresponds to a value of $\Gamma^* = 0.57$, substantially lower than the more classical form of the Kármán vortex at $N = 17$.

The corresponding patterns of the instantaneous velocity field are shown in the bottom rows of images in figures 9(*a*) and 9(*b*). In general, the features of these velocity fields reinforce the foregoing observations of the vorticity distributions. The ingestion of fluid in the upstream direction towards the base of the cylinder is indicated at $N = 7$ by large velocity vectors in regions near the base. At $N = 11$, there is an upstream-oriented jet along the plane of symmetry of the wake; it corresponds to converging of the clusters of vorticity towards the centre of the wake. At $N = 17$ and 25, the regions of low velocity near the cylinder are of minimum extent, due to the very rapid formation of vortices adjacent to the cylinder surface. Particularly important is the velocity field adjacent to the base at $N = 17$. The counterclockwise swirl associated with the Kármán vortex from the bottom of the cylinder induces abrupt separation from the base and formation of the vortex of opposite sense described in the foregoing.

Viewing the transient process of figures 9(*a*) and 9(*b*) as a whole, the following simplified scenario occurs. First, at the onset of oscillation, the vorticity concentrations in the shear layers separating from the cylinder respond in a subharmonic alternating sense, where the larger-scale concentrations of vorticity are formed from small-scale shear-layer vortices. This process continues until the separating layers from the cylinders are deflected inwards towards the plane of symmetry (see $N = 11$), forming a jet directed towards the base of the cylinder. This instant marks an important transformation in the structure of the near wake. After it occurs, formation of large-scale vortices tends to occur immediately downstream of the base. Following abrupt separation and vortex formation from the base of the cylinder ($N = 17$), induced by a Kármán vortex, a limit-cycle oscillation occurs, whereby the large-scale Kármán vortices are formed immediately adjacent to the base of the cylinder.

The shear layers separating from the surface of the cylinder are often viewed as equivalent to classical isolated mixing layers generated from, for example, a thin splitter plate. The mean velocity distributions across separated layers from a stationary cylinder, as well as the nature of disturbance amplification in these layers, are addressed by Unal & Rockwell (1988) and Khor & Sheridan (1994). These layers do indeed exhibit several features in common with simple mixing layers, provided the Reynolds number lies in the range such that Kármán vortex formation occurs

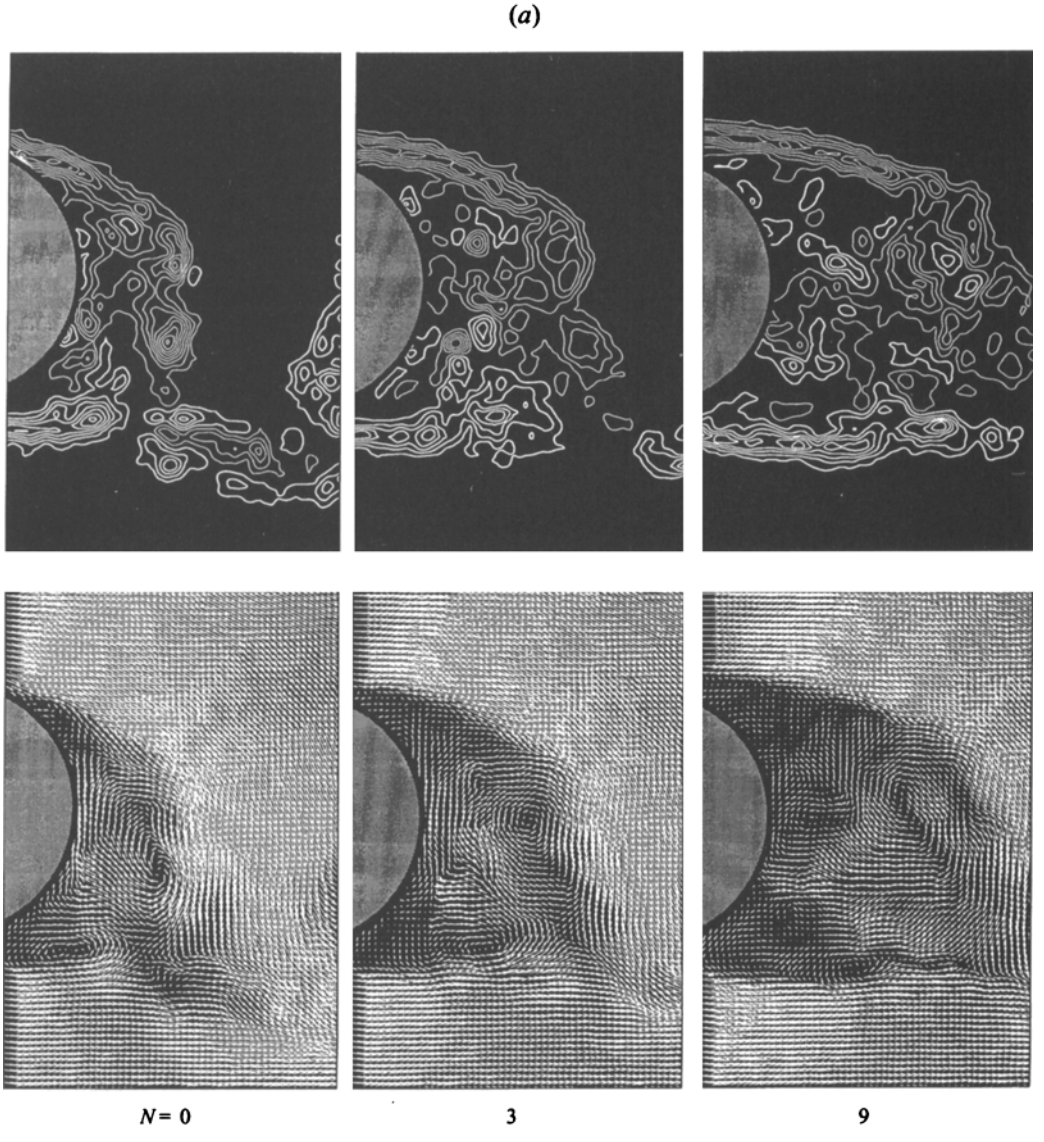

FIGURE 10(*a*). For caption see facing page.

sufficiently far downstream. It is evident from the present study, however, that the onset of perturbations of the cylinder, which initially induces vortex pairing similar to that in a simple mixing layer, eventually generates a state of the layer distinctly different from its isolated counterpart. The entrainment demands of these perturbed layers induce, with increasing time, drastic modifications of the flow in the base region of the cylinder, leading to a succession of complex states. Irrespective of the particular set of states observed during this transformation, the end consequence is a persistent and highly repetitive formation of Kármán vortices close to the base of the cylinder. This suggests that, once the velocity field in the very near-wake region is altered through formation of the small- and intermediate-scale vortical structures, it allows onset of an absolutely unstable disturbance amplification, leading to the limit-cycle oscillations of the large-scale Kármán vortices.

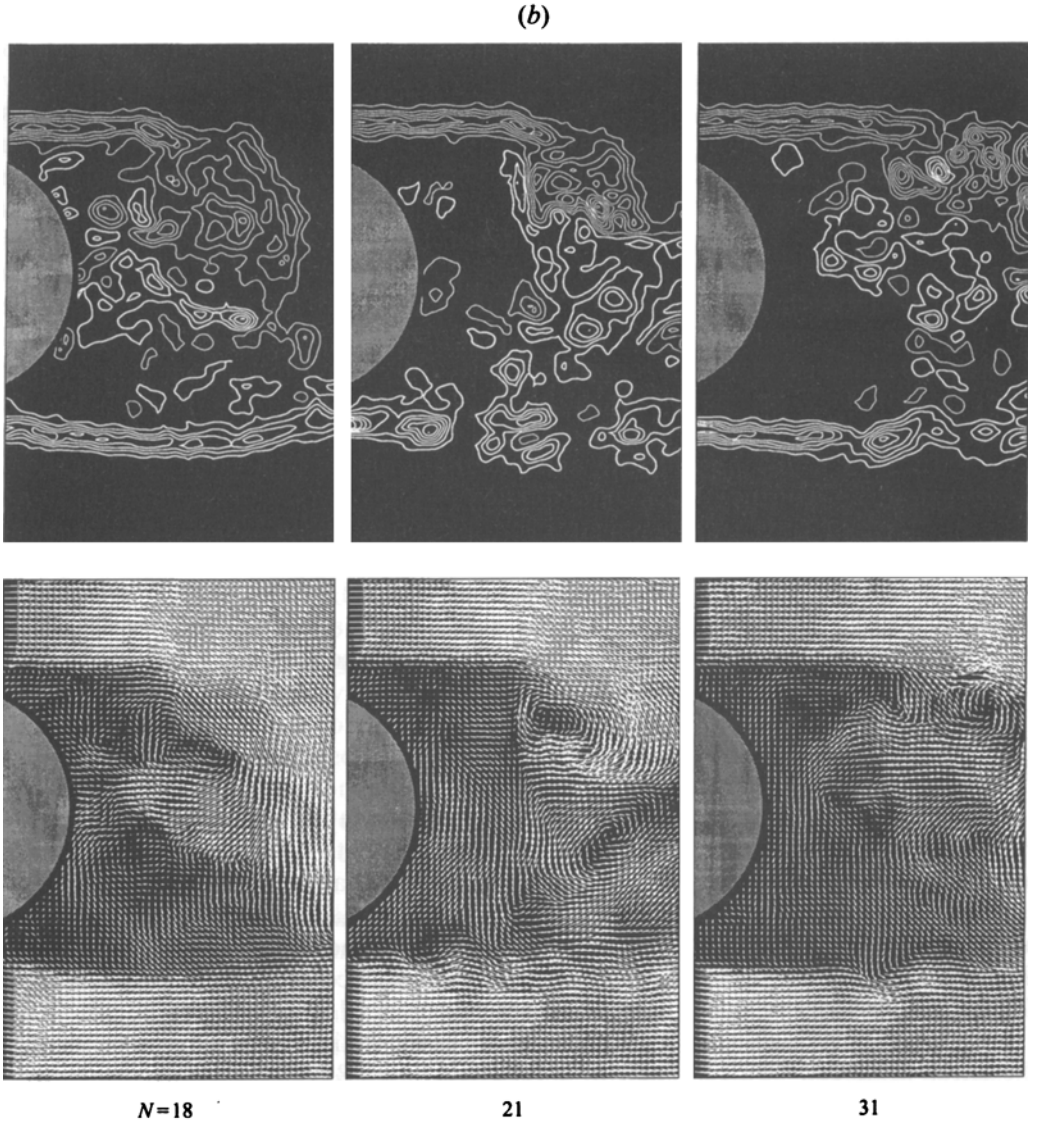

FIGURE 10. Transient response to cessation of cylinder perturbation. Excitation is at $f_e/f_i = \frac{1}{2}$, corresponding to $f_e/f_K = 3.35$, and $A/D = 0.04$. Top row: instantaneous vorticity fields. Bottom row: instantaneous velocity fields. $|\omega_{min}| = 5\ s^{-1}$, $\Delta\omega = 7.5\ s^{-1}$. $Re = 5000$. (*a*) $N = 0$, 3 and 9; (*b*) $N = 18$, 21 and 31.

4.7. *Transient response to cessation of cylinder perturbations: relaxation of near-wake*

When the periodic motion of the cylinder is abruptly terminated, the near wake relaxes to its undisturbed asymptotic form through a series of distinctive states. To examine this relaxation process, the steady-state response of the near wake is first attained. It corresponds to image $N = 25$ in figure 9(*b*). Then, the cylinder motion is abruptly terminated, represented by $N = 0$ in figure 10(*a*). In describing this evolution of the near wake, we focus on the large-scale vortex formed from the upper surface of the cylinder. For the images $N = 3$ and 9 in the top row of figure 10(*a*), the

instantaneous distributions of vorticity indicate that the vorticity layer from the top surface of the cylinder experiences an increase in radius of curvature, i.e. it tends to flatten out. Correspondingly, the large-scale cluster of negative (thin lines) vorticity moves further downstream. At $N = 9$, the large cluster of negative vorticity extends well across the wake and nearly intercepts the positive layer of vorticity from the bottom surface of the cylinder. At the larger values of $N = 18$–31, shown in figure 10(*b*), the initial region of the vorticity layer from the top shoulder of the cylinder is now essentially flat, i.e. parallel to the incident free stream, and the large cluster of negative vorticity extends only a limited distance across the wake, i.e. approximately to the plane of symmetry of the wake region. At the still larger value of $N = 31$, the region near the base of the cylinder is increasingly devoid of patches of vorticity, and the pattern of the near-wake structure tends toward the asymptotic undisturbed state shown in figure 5(*a*) at $A/D = 0$. These central features of the near-wake relaxation are also exhibited in the corresponding velocity fields in figure 10(*a*, *b*). The upstream-oriented jet-like flow near the plane of symmetry of the base region at $N = 18$ marks the onset of downstream migration of patches of vorticity in the base region, evident in images $N = 21$ and 31.

Particularly remarkable, however, is the relatively large number of cycles required for the wake to relax to its asymptotic undisturbed state. Even a time span corresponding to thirty-one cycles ($N = 31$), representing approximately nine cycles of the Kármán formation, are not adequate to completely achieve the undisturbed state shown in figure 5(*a*).

5. Concluding remarks

Excitation of the separated shear layers by perturbations of the cylinder is an effective means of indirectly controlling the development of Kármán vortices in the near wake, both for steady-state and transient perturbations of the cylinder. This control can be achieved at the fundamental and subharmonic frequencies of the unstable shear layer. Certain features of the shear-layer and near-wake response mimic those arising from increased Reynolds number in absence of cylinder perturbations. The central findings of this investigation are summarized as follows:

(*a*) The onset of highly concentrated vortices in the initial region of development of the shear layer can be postponed to a relatively high Reynolds number in a quiet facility. Even though instantaneous images show detectable regions of spatially periodic vorticity (at $Re = 5000$ in the present case), they have a low value of dimensionless vorticity concentration, defined as the ratio of the maximum instantaneous to averaged vorticity, $\omega_{max}/\Omega_{max} \approx 0.1$. Doubling the Reynolds number (to $Re = 10000$) increases $\omega_{max}/\Omega_{max}$ by a factor of about 5, accompanied by a fourfold increase in the instantaneous Reynolds stress. Correspondingly, the formation decreases substantially.

(*b*) The onset, degree of vorticity concentration, and circulation of the shear-layer vortices must be interpreted with caution, in view of the range of possible values of $\omega_{max}/\Omega_{max}$. Visualization techniques that yield streamlines can provide indications counter to those based on the actual patterns of vorticity. In the laboratory frame, regions of highly concentrated vorticity at small wavelength do not indicate well-defined spiral streamline patterns and corresponding foci of vortices, whereas weakly concentrated patterns of vorticity at larger wavelength do, even though both of these extreme cases have the same dimensionless circulation, normalized by the wavelength between vorticity concentrations. Moreover, the substantially different values of dimensionless vorticity concentration $\omega_{max}/\Omega_{max}$ for these two extreme cases will give

regions of locally injected marker in the form of streaklines which have a spatial extent counter to that of the concentrated vorticity.

(*c*) The onset of highly concentrated vortices in the shear layer can be induced and advanced upstream, in a deterministic and consistent manner, by cylinder displacement and velocity perturbations as small as $A/D = 10^{-3}$ and $v_e/U = 6 \times 10^{-3}$ respectively, even at relatively high Reynolds number. This highly sensitive response indicates that the separated shear layer is convectively unstable.

(*d*) The formation length of the first highly concentrated vortex in the shear layer decreases with increasing excitation amplitude A/D until a limiting position is attained. At this value of A/D, the initially formed vortex exhibits a change in timing, i.e. it switches from one side of the cylinder to the other. These alterations in the shear layer are accompanied by changes in the region between them: patches of vorticity migrate upstream towards the base. This process involves a decrease of formation length of the first Kármán vortex.

(*e*) The streamline topology of the shear-layer vortices, formed in the initial region of the separating shear layers shows, at small values of amplitude A/D, predominantly a stable focus, corresponding to spanwise stretching of the vortex. At larger values of A/D, however, more complex topology involving limit-cycle streamlines sets in. The corresponding topology in the base region between the layers, at small A/D, generally takes the form of diverging non-spiralling streamlines due to the entrainment demands of the separated layers. At large values of A/D, the streamlines transform to limit-cycle patterns associated with early formation of the Kármán vortices, and the associated saddle point systematically rotates with increasing A/D.

(*f*) Modulated, but ordered, patterns of shear-layer vortices can be induced even when the cylinder perturbation is sinusoidal. In turn, these modulated patterns induce relatively large-amplitude modulations of the initially formed Kármán vortices.

(*g*) Locked-in (phase-locked) patterns of shear-layer vortices promote rapid development of the Kármán vortices. The pattern of initially formed shear-layer vortices tends to remain spatially stationary, while the Kármán vortex develops spatially and temporally upon this pattern.

(*h*) Transient development of patterns of shear-layer vortices, induced by abrupt onset of periodic motion of the cylinder, involves a series of well-defined states, which allow the near-wake to transform from a system of perturbed mixing layers to well-defined Kármán vortices. Two critical states occur during this transformation: (i) a jet-like flow towards the base of the cylinder, which represents the first phase of formation of the Kármán vortices; and (ii) vortex formation from the base of the cylinder, induced by the Kármán vortex. After this second state is attained, a steady-state limit cycle occurs, involving Kármán vortex formation immediately adjacent to the base.

(*i*) Recovery from Kármán vortex formation towards a system of separated mixing layers is achieved by abrupt cessation of the periodic motion of the cylinder. The relaxation time is, however, very long, requiring more than thirty-one periods of the shear-layer instability, corresponding to nine cycles of the Kármán mode.

The authors gratefully acknowledge insightful discussions with Dr Jung-Chang Lin of Lehigh and Dr John Sheridan of Monash University, Melbourne, Australia during his sabbatical at Lehigh. Dr Lin also provided substantial support during the quantitative evaluation of images. Financial support was provided by the Office of Naval Research under Grants N00014-94-1-0185 and N00014-90-J-1510 and the National Science Foundation with Grants CTS-8922095 and CTS-9422432.

REFERENCES

AHMED, A., KHAN, M. J. & BAYS-MUCHMORE, B. 1993 Experimental investigation of a three-dimensional bluff-body wake. *AIAA J.* **31**, 559–563.

BEARMAN, P. W. 1967 On vortex street wakes. *J. Fluid Mech.* **24**, 625–641.

BEARMAN, P. W. & OBASAJU, E. D. 1982 An experimental study of pressure fluctuation on fixed and oscillating square-section cylinders. *J. Fluid Mech.* **119**, 297–321.

BLOOR, M. S. 1964 The transition to turbulence in the wake of a circular cylinder. *J. Fluid Mech.* **19**, 290–304.

BLOOR, M. G. & GERRARD, J. H. 1966 Measurements on turbulent vortices in a cylinder wake. *Proc. R. Soc. Lond.* A **294**, 319–342.

CHYU, C.-K. 1995 A study of the near-wake structure from a circular cylinder. PhD Dissertation, Department of Mechanical Engineering and Mechanics, Lehigh University.

CHYU, C.-K., LIN, J.-C., SHERIDAN, J. & ROCKWELL, D. 1995 Kármán vortex formation from a cylinder: role of phase-locked Kelvin–Helmholtz vortices. *Phys. Fluids* **7**, 2288–2290.

CHYU, C.-K. & ROCKWELL, D. 1996 Kármán vortex development: relation to symmetry of transition waves. *AIAA J.* (in press).

FILLER, J. R., MARSTON, P. L. & MIH, W. C. 1991 Response of the shear layer separating from a circular cylinder to small-amplitude rotational oscillations. *J. Fluid Mech.* **231**, 481–499.

GERRARD, J. H. 1965 A disturbance-sensitive Reynolds number range of flow past a circular cylinder. *J. Fluid Mech.* **22**, 187–196.

GERRARD, J. H. 1966 The mechanics of the formation region of vortices behind bluff-bodies. *J. Fluid Mech.* **25**, 401–403.

GERRARD, J. H. 1978 The wakes of cylindrical bluff body at low Reynolds number. *Phil. Trans. R. Soc. Lond.* A **288**, 351–382.

GREEN, R. B. & GERRARD, J. H. 1993 Vorticity measurements in the near wake of a circular cylinder at low Reynolds numbers. *J. Fluid Mech.* **246**, 675–691.

GRIFFIN, O. M. 1995 A note on bluff body vortex formation. *J. Fluid Mech.* **284**, 217–224.

GURSUL, I. & ROCKWELL, D. 1991 Effect of concentration of vorticity on streakline patterns. *Exps. Fluids* **10**, 294–296.

HO, C. M. & HUANG, P. 1982 Subharmonics and vortex merging in mixing layers. *J. Fluid Mech.* **119**, 443–473.

HUERRE, P. & MONKEWITZ, P. A. 1990 Local and global instabilities in spatially-developing flows. *Ann. Rev. Fluid Mech.* **22**, 473–537.

KHOR, M. & SHERIDAN, J. 1994 Characterization of the separated shear layer in the near-wake of a circular cylinder. *Intl Colloq. on Jets, Wakes and Shear Layers, Melbourne, Australia, 18–20, April.*

KOURTA, A., BOISSON, H. C., CHASSING, P. & HA MINH, H. 1987 Nonlinear interaction and the transition to turbulence in the wake of a circular cylinder. *J. Fluid Mech.* **81**, 141–161.

LIN, J.-C., TOWFIGHI, J. & ROCKWELL, D. 1995 Instantaneous structure of near-wake of a circular cylinder: on the effect of Reynolds number. *J. Fluids Struct.* **9**, 409–418.

MCCROSKEY, W. J. 1977 Some current research in unsteady fluid dynamics – the 1976 Freeman Scholar Lecture. *Trans. ASME I: J. Fluids Engng* **99**, 8–39.

NAKANO, M. & ROCKWELL, D. 1993 The wake from a cylinder subjected to amplitude-modulated excitation. *J. Fluid Mech.* **247**, 79–110.

NAKANO, M. & ROCKWELL, D. 1994 Flow structure in the frequency-modulated wake of a cylinder. *J. Fluid Mech.* **266**, 93–119.

ÖNGOEREN, A. & ROCKWELL, D. 1988 Flow structure from an oscillating cylinder. Part 1. Mechanisms of phase shift and recovery of the near-wake. *J. Fluid Mech.* **191**, 197–245.

PERRY, A. E., CHONG, M. S. & LIM, T. T. 1982 The vortex shedding process behind two-dimensional bluff bodies. *J. Fluid Mech.* **116**, 77–90.

PRASAD, A. & WILLIAMSON, C. H. K. 1996 The instability of the separated shear layer from a bluff body. *Phys. Fluids* **8**, 1347–1349.

ROCKWELL, D. & LIN, J.-C. 1993 Quantitative interpretation of complex, unsteady flows via high

image-density particle image velocimetry. *Optical Diagnostics in Fluid and Thermal Flow, Proc. SPIE – The Intl Soc. for Optical Engng*, vol. 2005, pp. 490–503.

ROCKWELL, D., MAGNESS, C., TOWFIGHI, J., AKIN, O. & CORCORAN, T. 1993 High-image-density particle image velocimetry using laser scanning techniques. *Exps. Fluids* **14**, 181–192.

ROCKWELL, D., TOWFIGHI, J., MAGNESS, C., AKIN, O., CORCORAN, T., ROBINSON, O. & GU, W. 1992 Instantaneous structure of unsteady separated flows via particle image velocimetry. *Rep.* PI-1. Fluid Mechanics Laboratories, Department of Mechanical Engineering and Mechanics, Lehigh University.

ROSHKO, A. & FISZDON, W. 1969 On the persistence of transition in the near-wake. In *Problems of Hydrodynamics and Continuum Mechanics*, pp. 606–616. SIAM.

SCHILLER, L. & LINKE, W. 1933 Druck- und reibungswiderstand des zylinders bei Reynoldsschen zahlen 5,000 bis 40,000. *Z. Flugtech. Motorluftschiffahrt* **24** (7), 193–198. (English transl. Pressure and Frictional Resistance of a Cylinder at Reynolds Numbers 5,000 to 40,000. *Natl Advisory Committee Aeronautics, Tech. Mem.* 715, July 1933.)

SHERIDAN, J., SORIA, J., JIE, WU & WELSH, M. C. 1993 The Kelvin–Helmholtz instability of the separated shear layer from a circular cylinder. In *Bluff-Body Wakes, Dynamics and Instabilities* (ed. H. Eckelmann, J. M. Graham, P. Huerre & P. A. Monkewitz). *Proc. IUTAM Symp. Göttingen, Germany, September 7–11, 1992*, pp. 115–117. Springer.

STUART, J. T. 1967 On finite amplitude oscillations in laminar mixing layers. *J. Fluid Mech.* **29**, 417–440.

SZEPESSY, S. & BEARMAN, P. W. 1992 Aspect ratio and end plate effects on vortex shedding from a circular cylinder. *J. Fluid Mech.* **234**, 191–217.

UNAL, M. F. & ROCKWELL, D. 1988 On vortex formation from a cylinder. Part 1. The initial instability. *J. Fluid Mech.* **190**, 491–512.

WEI, T. & SMITH, C. R. 1986 Secondary vortices in the wake of circular cylinders. *J. Fluid Mech.* **169**, 513–533.

WILLIAMSON, C. H. K. 1996 Vortex dynamics in the cylinder wake. *Ann. Rev. Fluid Mech.* **28**, 477–539.

WILLIAMSON, C. H. K. & ROSHKO, A. 1988 Vortex formation in the wake of an oscillating cylinder. *J. Fluids Struct.* **2**, 355–381.

ZDRAVKOVICH, M. M. 1982 Modification of vortex shedding in the synchronization range. *Trans. ASME I: J. Fluids Engng* **104**, 513–517.